11

PMM/I - 279

COMISION NACIONAL DE ENERGIA ATOMICA
PRESIDENCIA DE LA NACION

PROYECTO MULTINACIONAL DE METALURGIA
(Programa Regional de Desarrollo Científico y Tecnológico)

y

PROYECTO DE TECNOLOGIA DE LA SOLDADURA
SECYT – CNEA

TOPICS ON WELD METAL METALLURGY

Trabajos realizados por el Grupo de Tecnología de la Soldadura
División Fundición y Solidificación
Departamento de Materiales

Gerencia de Desarrollo
Buenos Aires - Argentina
1980

PMM/I - 279

COMISION NACIONAL DE ENERGIA ATOMICA
PRESIDENCIA DE LA NACION

PROYECTO MULTINACIONAL DE METALURGIA
(Programa Regional de Desarrollo Científico y Tecnológico)

y

PROYECTO DE TECNOLOGIA DE LA SOLDADURA
SECYT — CNEA

TOPICS ON WELD METAL METALLURGY

Trabajos realizados por el Grupo de Tecnología de la Soldadura
División Fundición y Solidificación
Departamento de Materiales

Gerencia de Desarrollo
Buenos Aires - Argentina
1980

INDEX

"THE EFFECT OF WIRE FEED SPEED ON THE STRUCTURE IN ELECTROSLAG WELDING OF LOW CARBON STEEL"

by M. Solari and H. Biloni

The Effect of Wire Feed Speed on the Structure in Electroslag Welding of Low Carbon Steel

Increasing wire or electrode feed rate at constant voltage has no significant effect on penetration but increases pool depth and decreases the shape factor, while increasing welding voltage at constant electrode feed rate increases both pool depth and penetration but has little effect on the shape factor

BY M. SOLARI AND H. BILONI

ABSTRACT. In Electroslag welding of low carbon steel, the effects of electrode feed rate on weld geometry, welding velocity, energy input, weld macrostructure and the microstructure of the weld and HAZ were determined. Results showed that increasing the electrode feed rate at constant voltage had no significant effect on the penetration but increased the pool depth, decreased the shape factor and increased the encounter angle. The pool shape was approximately a paraboloid of revolution. Increasing the welding voltage at constant feed rate increased both pool depth and penetration, but had little effect on the shape factor.

Standard and special metallographic etchants were used to study the transition region between the weld and the base metal, the average dendritic cell diameter, the pool shape and the mechanism of metal transfer from the base metal to the liquid pool as a function of the penetration; results were related to the welding parameters.

Introduction

During the past few years, numerous papers describing the details of electroslag welding (ESW) have been published.[1-5] Essentially, ESW is an automatic arcless welding process, best suited for the joining of plate 2 in. (5 cm) or thicker. Joule heating of an electrically conductive pool of molten slag serves to melt the filler metal together with a portion of the base metal on either side of the joint. The resulting weld pool and the overlying pool of molten slag are contained within the joint by water-cooled copper shoes.

The geometry of the system is such that the solid-liquid interface beneath the weld pool soon assumes a dynamically stable shape which is determined by a combination of welding variables, joint separation, and plate thickness. Once dynamic equilibrium is achieved, the solidification rate and the temperature gradient at the solid-liquid interface depend upon the location on the interface but are independent of time, providing the welding conditions are not changed.

The microstructure of solidified weld metal is known to have a strong influence on the mechanical, physical and chemical properties of the weld.[6-8] The shape of the molten weld pool and the rate of growth at the solid-liquid interface affect both the size and shape of the grains, their relative crystallographic orientation, and both macro- and microsegregation. In electroslag welding, it is possible to define an "encounter angle" which depends upon the shape and depth of the weld pool and affects the sensitivity to centerline hot cracking.[1]

Although it is not possible to observe the shape of the pool during welding, several theoretical and experimental methods have been developed to overcome this difficulty. Essentially, the experimental methods are intended to reveal the position of the S-L interface using different tracers, such as radioactive materials and sulfur additions subsequently revealed by sulfur prints.[9] These methods reveal the shape of the pool at certain moments of the process. On the other hand, theoretical methods have been used by several authors in order to obtain expressions for predicting the pool shape; these are used not only in welding but also in other processes, such as the electroslag remelting process (ESR), which has similar thermal characteristics.[10,11] The mathematical problem is complex enough to require the introduction of several simplifications in order to obtain formal expressions able to describe the pool. A subsequent work will describe a simplified model of the thermal field existing during the electroslag welding operation.

Savage and co-workers have done

M. SOLARI is with the Department of Materials and H. BILONI is Head of the Solidification and Casting Division, Comision Nacional de Energia Atomica, Buenos Aires, Argentina.

extensive studies[8-12,43] on the correlation between welding structures and substructures and the operational variables of different welding processes. The aim of their type of approach is to provide correlations between solidification and phase transformation structures and substructures and the mechanical properties of the weld.

The work described in this paper corresponds to the initiation of studies on the ESW process at the Solidification and Casting Division of the Atomic Energy Commission of Argentina. Its principal goal is to determine the effect of electrode feed rate on the geometry of the weld pool, the welding speed, the energy input and the resultant macro- and microstructure of the weld and HAZ. Different techniques were used in order to reveal the pool shape. In addition, the mechanisms involved in the material transfer from the base metal to the weld region were to be studied.

Carbon steel was used in the experiments in order to develop an improved understanding of both the solidification substructures and the microstructure present in the HAZ region. The results obtained during this research were correlated with the experience accumulated in the laboratory as a result of extensive studies on controlled solidification performed in the past.[14,15]

Experimental Procedure

Equipment

A commercial constant potential dc welding power supply with nominal outputs of 85, 58 and 35 V was used in the reverse polarity mode. The maximum current was varied between 1000 and 1200 A. The equipment enables the use of either one or two electrodes according to the plate thickness; the electrodes can be used with or without oscillation.

Table 1—Chemical Compositions of Base Metal, Electrode, Consumable Guide and Typical Weld Deposit, Wt-%[16]

	C	Mn	Si	S	P
Base metal	.07	.48	.05	.039	.012
Consumable guide	.19	.65	.12	.018	.011
Electrode	.09	1.15	.54	.016	.020
Weld deposit*	.11	.79	.24	.030	.016

*Balance is Fe.

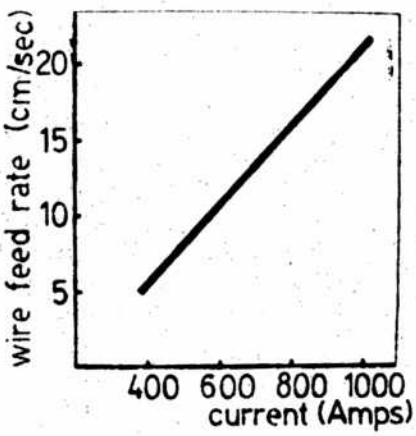

Fig. 1—Relationship between V_e and I for electrode of 0.238 cm diameter.

Material

The chemical composition of the plate, electrode feed and consumable guide used are given in Table 1. The flux used had the following composition: SiO_2—36.29%; MnO_2—27.37%; CaO—16.82%; Al_2O_3—8.72%; MgO—2.67%; TiO_2—2.53%; Fe_2O_3—1.27%; Na_2O—0.93%; K_2O—0.72%.

Welding Procedure

Complete details of welding conditions have been given in previous papers.[16,17] They can be summarized as follows:

1. Constants: Plate size was 35 × 35 × 5.1 cm (13.8 × 13.8 × 2 in.) and the separation between plates to be welded was 2.5 cm (1 in.) at the bottom and 3.0 cm (1.18 in.) at the top, regardless of the plate height. A nominal value of 2.8 cm (1.1 in.) was used in welding velocity calculations. A 0.238 cm (3/32 in.) diameter commercial electrode and one consumable guide were used without oscillation. Slag depth was maintained constant by addition of flux during the operation. A constant voltage of 40 V was used.

2. Welding Speeds and Resulting Weld Currents: The independent variable studied was electrode feed rate V_e over the range from 5 to 19 cm/sec (approx. 2-7.5 ips). This variable controls welding current. Figure 1 shows the relationship between electrode (i.e., wire) feed rate V_e, and weld current, I.

Several factors, such as minor variations in the slag level, periodic fluctuation of the electrode feed rate and stray arcs, caused fluctuations of ± 50 A in the measured weld current.

Measurement of Weld Geometry

Figure 2 shows schematically the metallographic planes upon which the structural analyses were made. The surfaces were prepared by standard mechanical polishing techniques. In order to measure the geometry of the welds, both metallographic and sulfur addition techniques were used.

Metallography. The composition of the etchant was $CuCl_2$—45 g; $FeCl_3$—8 g; HCl—180 cc; HNO_3—1.5 cc; H_2O—180 cc; alcohol—380 cc. The etching was performed at room temperature. A subsequent light repolishing with alumina reveals the segregation and thus delineates the pool shape permitting the measurement of the depth of the pool H, the weld width b, and the "encounter angle" as shown schematically in Fig. 3. The same etching procedure was also used in order to reveal the segregation substructure.

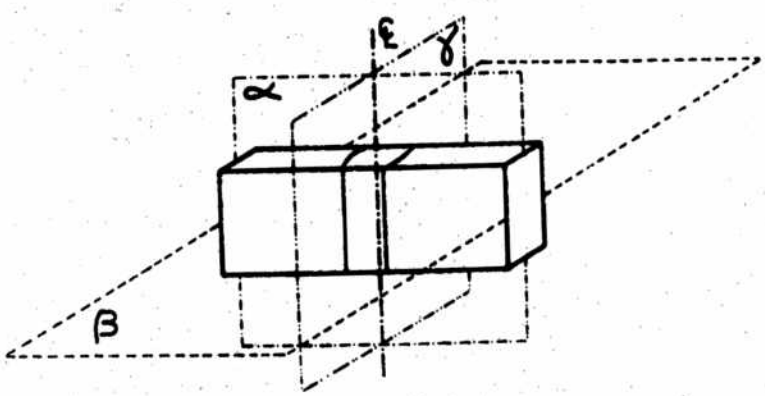

Fig. 2—Schematic representation of the sections metallographically analyzed: α = vertical plane through the midsection of the plate; β = vertical plane through the midsection of the weld and perpendicular to plate surfaces; γ = horizontal cross section of the weld

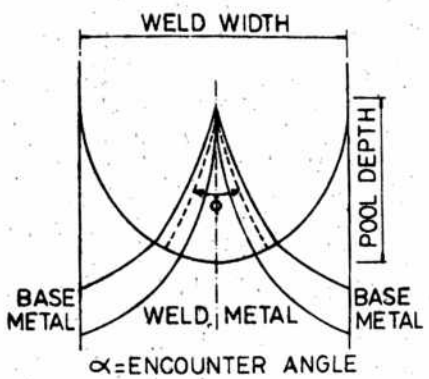

Fig. 3—Schematic representation of a section on plane α; the pool depth H, the weld width b_w and the "encounter angle" are defined

Sulfur Print Technique. In order to make periodic sulfur additions during welding, the insulating rings of the consumable guide were replaced by metallic rings containing 2 g of FeS. When the molten slag reached the rings, the S was incorporated in the weld pool. After welding a sulfur print could then be prepared to reveal the pool profile.

A shape factor* ($\delta = b_w/H$) was calculated; this is considered to be an important parameter influencing the susceptibility to crack formation.[1]

Calculation of Energy Input

The travel speed, V_w, was calculated as follows:

$$V_w = (A_e/A_g) \times V_e$$

A_e is the cross sectional area of the electrode; A_g is the cross sectional area of the gap between the plates to be welded and V_e is the electrode feed rate.

The error involved was estimated as 4%. The most important source of error was the difference between the actual value of A_g and the calculated value with the nominal plate separation, b_g.

The energy input was then calculated as follows:

$$\text{E.I.} = \frac{\text{Volts} \times \text{Current} \times 60}{\text{travel speed (in ipm)} \times 1000} = \text{kJoules/in.}$$

$$\text{and: kJ/cm} = (\text{kJ/in.}) \times 0.394$$

Metallographic Procedures

Macrographic Examination. Both 10% nital and the previously mentioned etchant were used. Either etchant allows the measurement of the encounter angle on the α plane (refer to Fig. 2). The dilution of the weld metal with base metal was measured on the β plane and calculated by means of the expression:

$$D = ((A_w - A_g)/A_w) \times 100$$

where A_w is the cross sectional area of the weld and A_g is the cross sectional area of the original gap between the plates to be welded.

Metallographic Examination. In order to reveal the microstructure and the solidification substructure, two etchants were used: nital 1% and a reagent with the following composition: Cu_2Cl_2–45 g; $FeCl_2$–8 g; HCl–180 cc; HNO_3–2 cc; H_2O–180 cc; alcohol–380 cc. Etching was performed at room temperature.

Both etchants, together with the etchant used to detect the shape of the weld pool, were used in order to study the transition zone between the weld metal and the HAZ, as well as the mechanism involved in the metal transfer from the base metal to the weld pool.

Results and Discussion

Table 3 summarizes the experiments performed and the welding conditions, as well as the calculated and measured dependent variables.

Table 2–Welding Procedures

Plate thickness	5.1 cm (2 in.)
Plate separation	2.8 cm (nominal) (1.10 in.)
Electrode diameter	.238 cm (3/32 in.)
Oscillation	none
Number of electrodes	One
Depth of slag pool	4.0 cm (1.57 in.)
Voltage	40 V (open circuit)
Current	450-900 A
Electrode feed rate	5-19 cm/sec (118.11-448.82 ipm)

Effect of Electrode Feed Rate on the Shape of the Pool

Penetration. Table 3 shows that when the welding voltage was held constant the weld width was not greatly influenced by current changes within the range of electrode feed speed studied. Complementary experiments made with 35 and 55 V showed that the welding voltage is the major factor controlling the penetration.

The weld width, as measured on the α plane, is affected both by the slag depth and the energy input. Fluctuations in electrode feed rate were observed at electrode feed rates near the lower end of the range studied. These fluctuations caused variations in the energy input and thus caused corresponding changes in weld width.

This effect is shown in Fig. 4 where the appearance of the weld on the α plane is shown both schematically and by actual photomacrographs. In both instances the weld made with the low electrode feed rate is shown at the right. This behavior agrees with the mathematical conclusion that at constant power the penetration depth is most sensitive to welding speed variations at the low end of the travel speed range.[1]

Depth of Pool. Figure 5 is a photomacrograph of the α plane taken at ×6. It shows how the typical segregation substructure in the weld delineates the weld pool profile. Complementary to these observations, a sulfur addition was used in some experiments.

Figure 6 is a sulfur print taken of the α plane and shows how the dark, high sulfur region reveals the shape of the weld pool. A careful comparison between both techniques showed

*Symbolized here by Greek delta (δ) instead of normally used Greek psi.

Table 3–Welding Variables and Experimental Results

Experiment	Electrode feed rate, cm/s (in./s)	Current, A	Voltage, V	Travel speed, ipm	Energy input, kJ/in.	Encounter angle, deg	Pool depth H, cm	Pool depth H, (in.)	Weld width bw, cm	Weld width bw, (in.)	Shape factor, θ	HAZ width–locus of A_c, cm	HAZ width–locus of A_c, (in.)	Dilution D,%
1	7.0 (2.8)	450	40	0.48	2250	45	1.4	(0.55)	5.4	(2.13)	3.86	1.10	(0.433)	43
2	7.0 (2.8)	450	40	0.48	2250	35	1.3	(0.51)	5.0	(1.97)	3.85	1.18	(0.465)	–
3	7.0 (2.8)	450	40	0.48	2250	58	1.2	(0.47)	5.0	(1.97)	4.17	–		–
4	11.0 (4.3)	600	40	0.75	1920	–	2.6	(1.02)	5.9	(2.38)	2.27	1.40	(0.551)	43
5	13.5 (5.3)	700	40	0.92	1826	80	2.5	(0.98)	5.5	(2.17)	2.20	–		–
6	13.5 (5.3)	700	40	0.92	1826	83	2.6	(1.02)	5.9	(2.32)	2.27	1.25	(0.492)	–
7	19.0 (7.5)	900	40	1.30	1662	110	3.1	(1.22)	5.0	(1.97)	1.61	1.00	(0.394)	41
8	19.0 (7.5)	900	40	1.30	1662	92	3.8	(1.50)	5.4	(2.13)	1.42	0.95	(0.374)	37
9	19.0 (7.5)	900	40	1.30	1662	115	3.9	(1.54)	4.5	(1.77)	1.15	–		–
10	19.0 (7.5)	900	40	1.30	1662	120	3.3	(1.30)	6.0	(2.36)	1.82	–		–
Complementary experiments														
11	11.0 (4.3)	600	35	0.75	1680	60	1.8	(6.71)	4.2	(1.65)	2.33	1.15	(0.453)	–
12	11.0 (4.3)	600	55	0.75	2640	75	3.5	(1.38)	7.5	(2.95)	2.14	1.40	(0.551)	58

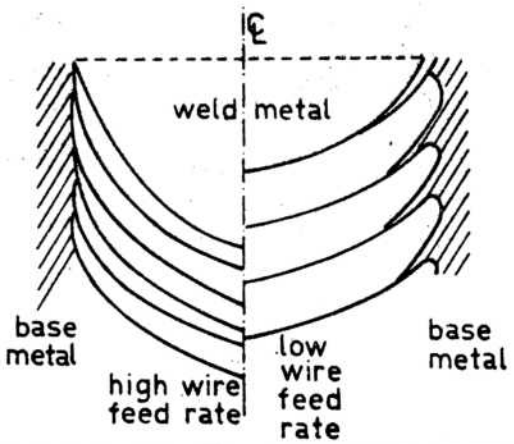

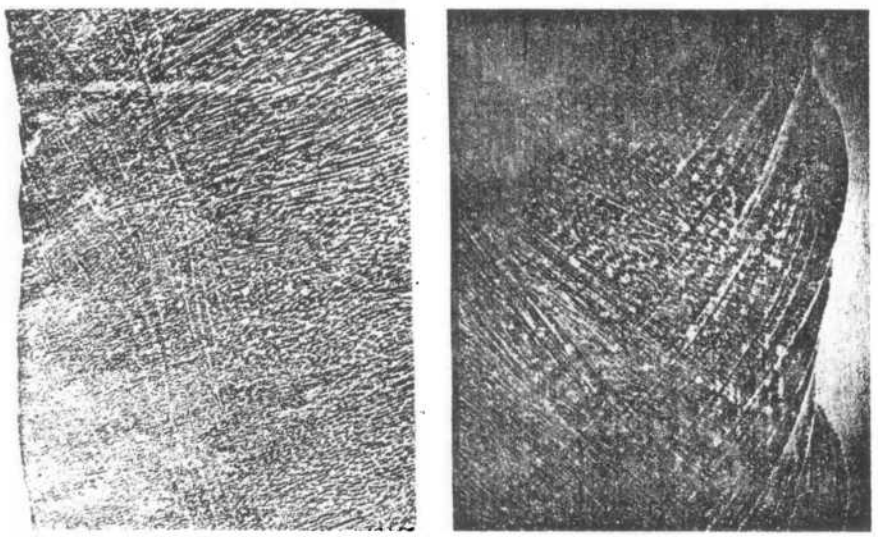

Fig. 4—a (top) Schematical representation of the penetration variation with the welding speed; b (bottom) variation of the penetration with the current intensity: experiment 1 (left) V = 40, I = 450 A; experiment 8 (right) V = 40, I = 900 A

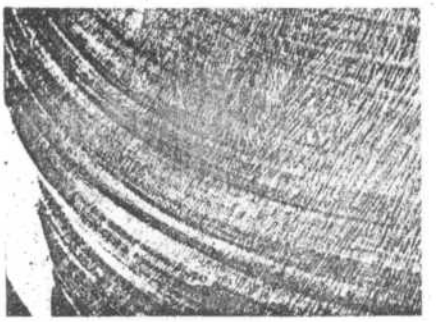

Fig. 5—Metallographic analysis of experiment 6. The etch reveals the segregation substructure and shows the pool shape. ×6 (reduced 50% on reproduction)

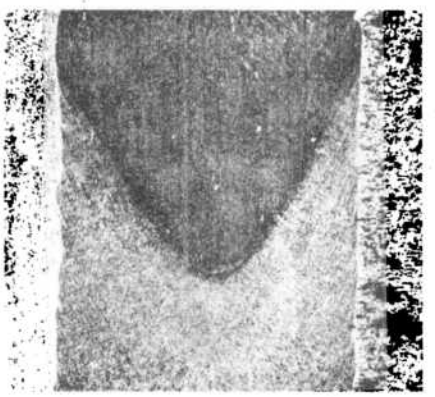

Fig. 6—Shape of the pool revealed in experiment 9 through a sulfur print

excellent agreement. Both techniques were able to reveal an increment in the pool depth H when the electrode feed rate was increased.

Shape Factor. δ is a useful parameter for describing the geometry of the liquid pool. The relative orientation of the grains, and therefore the encounter angle, can be related to the shape factor. Inspection of Table 3 indicates that at a constant voltage of 40 V the shape factor, δ, is inversely related to the electrode feed rate. Note that the shape factor varied from an average of 1.50 with an electrode feed rate of 19 cm/s (7.5 in./s) to about 4 with an electrode feed rate of 7 cm/sec (2.8 in./s).

The complementary experiments show that, when the electrode feed rate is held constant, the shape factor is essentially independent of the welding voltage.

Cross Sectional Area of the Pool. In general the weld pool has the shape of a somewhat distorted paraboloid of revolution. Figure 7 is a schematic showing the type of distortion of the solid liquid interface reported to be common in electroslag melting.[11] A similar distortion occurs near the center of an electroslag weld where a decrease in the rate of heat extraction caused by the increased length of the heat flow path results in a decrease in the growth rate at the solid liquid interface.

Referring again to Fig. 7 and recalling that the travel speed, V, is constant, since the growth rate R is given by $R = V \cos \theta$ a decrease in R must result in an increase in θ. This is shown schematically in Fig. 7 for the growth vectors R_1 and R_2 corresponding to the theoretical and actual growth conditions, respectively.

Figure 8 corresponds to another distortion which appears near the water cooled shoes. This distortion is accentuated by decreasing the pool depth. It is also related to the liquid flow within the weld pool.

Dilution. The calculated values of this parameter ranged from 39 to 58% and increased as the energy input increased.

Effect of Electrode Feed Rate on Welding Speed

For each experiment, the values of travel speed were calculated from electrode feed rate data. For this study, the travel speed ranged from 1.45×10^{-2} and 5.5×10^{-2} cm/s (0.34 and 1.30 ipm)—Table 3.

Effect of Electrode Feed Rate on Energy Input

At constant voltage and weld gap, the energy input is also determined by the electrode feed speed. At 40 V the energy input ranged from 2250 kJ/in. (886 kJ/cm) with 7 cm/sec electrode feed rate to 1662 kJ/in. (654 kJ/cm) with 19 cm/sec wire feed speed.

Effect of Electrode Feed Rate on Macrostructure

The columnar structure in the solidified metal of the weld originated both by epitaxial growth from the partially melted grains of the base metal and also by the nucleation on the refrigerated shoes. The grains grow in the easy growth direction which is most nearly parallel to the direction of heat extraction. Thus growth tends to occur approximately perpendicular to the surface of the pool. Consequently, the shape of the pool controls the angle of the grain growth direction with relation to the axis of the weld, and thus controls the value of the encounter angle.

The importance of the value taken by this angle arises from the fact that a

higher angle produces a greater centerline segregation and, as a consequence, a higher susceptibility of centerline hot cracking.[1] In the present work, encounter angles between 35 and 120 deg were observed. With constant voltage the smaller values correspond to the smaller electrode feed rate range (see Table 3). Figure 9 corresponds to a macrostructure on the β plane (refer to Fig. 2 for orientation) and shows a cross section of a fine columnar structure in a low carbon steel.

Effect of Electrode Feed Rate on Microstructure

Solidification Substructure. By applying special metallographic techniques, the structure and substructure of the weld have been investigated as well as the transition zone between the weld and the HAZ. At the same time, the mechanism of metal transfer from the base metal to the liquid pool can be understood by close examination of the segregation substructure.

Figures 10 and 11, obtained by metallographic etchants developed by Savage *et al*,[13] clearly show that, similar to other welding processes, the boundary between the two zones is not a line. Instead, it is a transition region composed of a zone melted without mixing and a partially melted zone identified by the segregation substructures clearly shown in Fig. 11. In that region, phases and inclusions of low melting point have been melted during the thermal cycle of the process.

The substructure of the weld metal in the 100% mixed region corresponds to a cellular dendritic type. For a constant energy input, the average cell spacing increased from the water cooled shoes or base metal to the weld centerline—Fig. 8. Decreasing the electrode feed rate causes the average cell spacing to increase throughout the weld due to the disminished cooling rate, as Fig. 12 clearly shows. This result agrees with the conclusion of other authors in the sense that the choice of welding conditions influences the pattern of microsegregation.[19]

Mechanism of Metal Transfer from the Base Metal to the Liquid Pool. The metallographic analysis with the different etchants used gives information about the mechanism of material transfer from the base metal to the molten pool.

In all the experiments carried out, the transition between weld and HAZ is characterized by a structure similar to that shown in Fig. 13a. Light etching projections entering the weld region with contour related to the shape of the pool appear at the base metal interface. These projections always had an etching behavior identical to that of the base metal. However, the same type of solidification substructure appears in both these projections and in the dark etching region of the weld, indicating that the segregated solidification substructures are common to both regions—Fig. 13b.

These results suggest that the projections are an extension of the unmixed melted zone.[20] However, the projections are more prominent when the travel speed is low. Figure 4 shows how the pool depth influences the formation of these projections. Note that at low electrode feed rates, and therefore at low travel speeds, the projections become longer and the weld interface more irregular in shape.

Some experiments in which the welding current was interrupted were helpful in understanding the mechanism of material transfer from the base metal to the weld pool. Figure 14 consists of α plane macrographs of two such welds showing the geometry of the slag-pool at the instant the current was interrupted. In each case the left hand side of the macrograph corresponds to the weld centerline. The weld at the left, which was made with 40 V and a travel speed of 1.22 cm/min (0.48 ipm), exhibited a shape factor of 4.17. That at the right was made with 55 V and a travel speed of 1.91 cm/min (0.75 ipm) and had a shape factor of 2.14.

In the weld with the higher shape factor (made with the lower travel speed), the slag pool encroaches upon the base metal to a greater degree and produces a pendulant overhang on which a layer of molten base metal adheres by surface tension.

Figure 15 shows, in schematic form, the mechanism proposed to explain the formation of the projections of unmixed molten base metal. First, the depth of the stagnant boundary layer (shown by the dashed line above the solid-liquid interface) is controlled by the amount of convective mixing in the liquid and is thus controlled by the depth of the molten pool and the

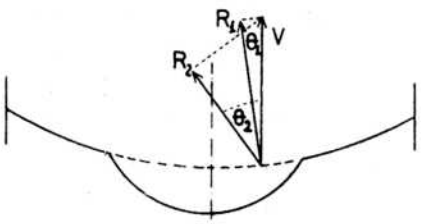

Fig. 7—Distortion of the pool shown schematically. The decrease in the rate of heat extraction at the central zone of the weld produces a decrease in R. As a consequence, θ increases in order to satisfy the expression $R = V \cos \theta$.

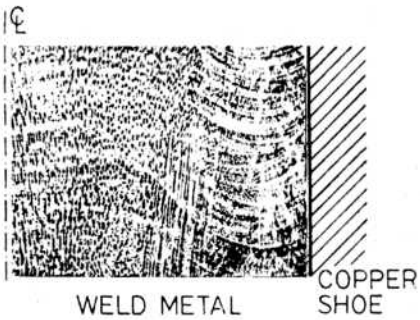

Fig. 8—Distortion near the refrigerated shoes revealed through metallographic etching—experiment 2. ×6 (reduced 75% on reproduction)

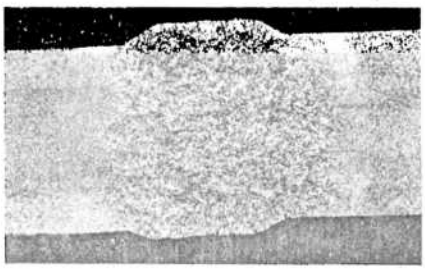

Fig. 9—Macrographic structure observed on plane β. Etching with nital reveals the structure of the weld and HAZ. Original reduction 30% (reduced 46% further on reproduction)

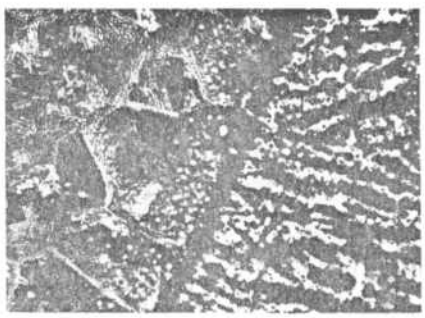

Fig. 10—Boundary between the weld and the HAZ. The segregated solidification substructure of the weld zone is noticeable and the partially melted zone is also revealed by the segregation substructure. ×100 (reduced 50% on reproduction)

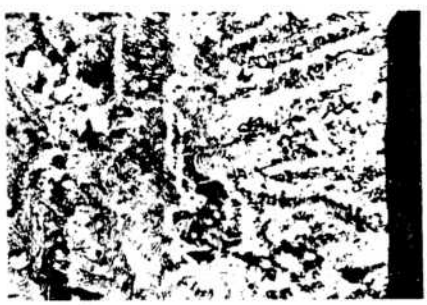

Fig. 11—Detail view of the weld interface showing the fusion zone and the partially melted zone. ×100 (reduced 50% on reproduction)

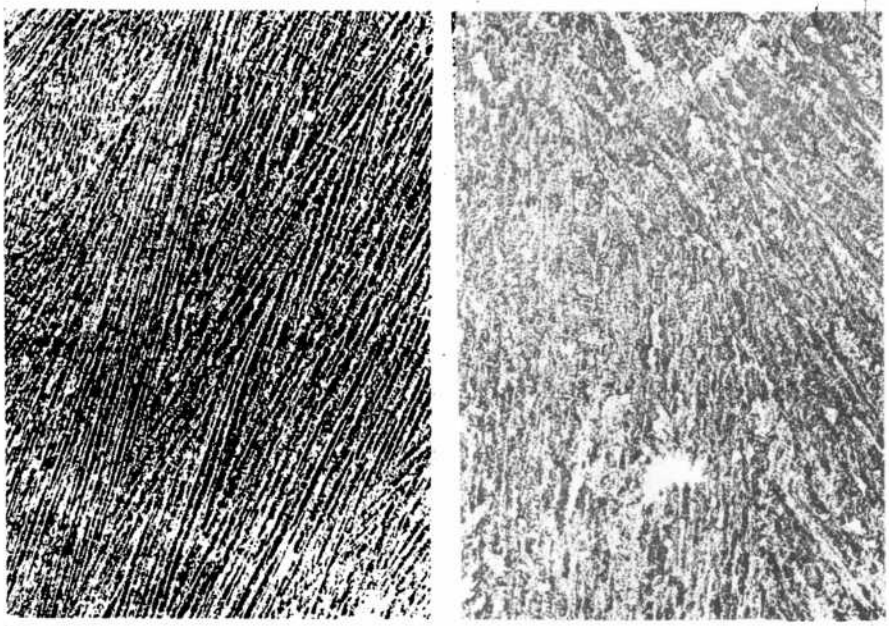

Fig. 12—Comparison between coarse (exp. 12) and fine (exp. 11) substructure of two welds made with different energy inputs. ×6 (reduced 50% on reproduction)

travel speed. In general, decreasing the pool depth, H, increases the thickness of the boundary layers and permits the layer of molten base metal (shown in black in Fig. 15) to slide under the stagnant layer periodically and thus form an unmixed projection of the type shown at right in Fig. 4b.

Increasing the travel speed both increases the depth of the pool H and the rate of solidification R. Increasing H decreases the thickness of the boundary layer owing to more effective convective mixing, and increasing R decreases the time available for the molten layer of base metal to slide into the weld pool. Thus, the projections become shorter and thinner as the travel speed is increased.

Encroachment of the slag pool into the base metal produces a pendulant overhang such as is indicated in Fig. 15 (and at the right in Fig. 14). When this occurs, the molten base metal adhering to the overhang can flow down the overhang, as indicated at A in Fig. 15, to form drops which ultimately are transferred to the liquid metal pool. In summary, for high penetration welds both mechanisms are operative, but for lower values of penetration, only the "projection" mechanism acts.

Welding HAZ Dimensions and Structure. The approximate gradient in the peak temperature experienced in the HAZ was determined from macrographs on the *a* plane similar to the one shown in Fig. 16. The fusion boundary is visible at the left and represents the locus of the region experiencing temperatures in excess of the liquidus. Near the center of Fig. 16, an abrupt transition occurs from an extremely fine grain size at the left to a coarser grain size at the right. This abrupt change in grain size identifies the locus of the region experiencing a peak temperature approximately equal to the A_{c1} transition temperature. Thus, by measuring the distance from the weld interface to this location, an indication of the effect of welding variables on the extent of the HAZ could be obtained.

From such measurements, the distance to the locus of the A_{c1} was found to vary from 0.95 cm (0.374 in.) for a weld made with an energy input of 1662 kJ/in. to a maximum of 1.4 cm (0.551 in.) for a weld made with an energy input of 2640 kJ/in. Table 3

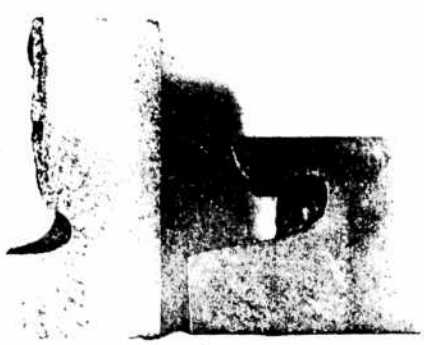

Fig. 14—Comparison of the shape of the welds on plane a for experiments 3 and 12 ×1.8 (reduced 51% on reproduction)

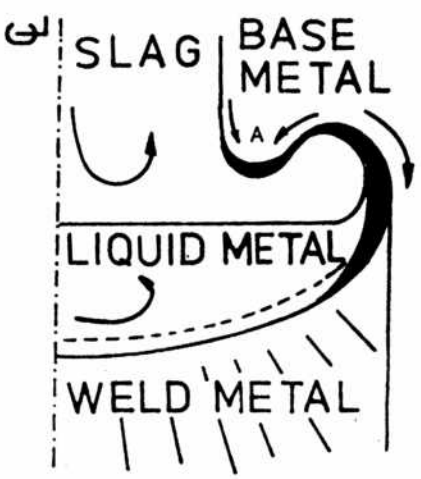

Fig. 15—Schematic representation of both mechanisms of metal transfer

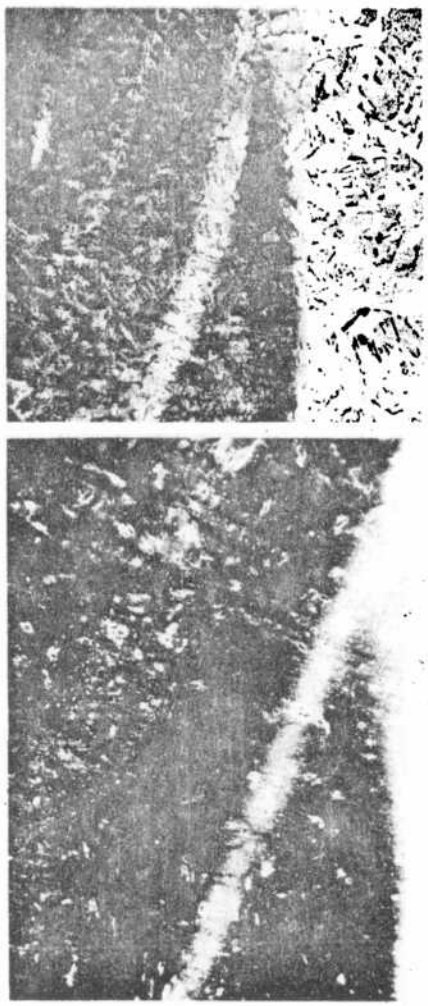

Fig. 13—Metallographic structure observed on plane a: a (top)—shows the projections of the unmixed fusion zone; b (bottom)—shows the presence of a segregated solidification substructure in the projections. ×100 (reduced 46% on reproduction)

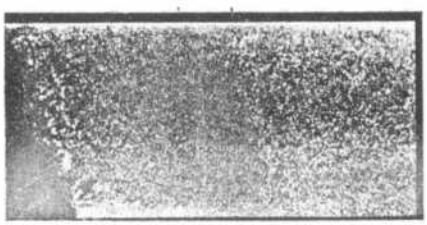

Fig. 16—Metallographic structure of the HAZ. Etching with nital reveals the weld metal, coarse grained region, refined zone, partially refined zone and unaffected base metal. ×6 (reduced 51% on reproduction)

summarizes these data in the next to the last column.

Conclusions

Macroscopic studies of the solidification structure in ESW of low carbon steel showed that when the electrode feed rate was increased at constant voltage:

1. The penetration remained approximately constant.
2. The pool depth increased.
3. The shape factor decreased.
4. The encounter angle increased.
5. The pool shape remained approximately a paraboloid of revolution.

Microscopic studies of the microstructure indicated that:

1. A transition zone at the edge of the weld consists of an unmixed molten zone and a partially melted zone.
2. By increasing the energy input the average dendritic cell diameter was increased.
3. Owing to fluctuations in the speed of the electrode feed, fluctuations in the specific power occur resulting in penetration variations and fluctuations of the solidification rate. These fluctuations can be detected metallographically by suitable etchants.
4. The fluctuations in the solidification rate cause transfer of molten base metal to the liquid pool by sliding through the stagnant boundary layer existing in contact with the S-L interface. This molten base metal does not mix with the rest of the liquid. As a consequence, it can be considered as a projection of the unmixed molten region. Increasing the pool depth and solidification rates decreased the length and thickness of the projections.
5. The mechanism of metal transfer from the base metal to the liquid pool depends upon the penetration of the slag pool into the base metal. In addition, when the penetration becomes large enough to produce a pendulant overhang in the base metal, molten droplets form and are transferred through the slag to the weld pool. At low travel speed both mechanisms are effective.

Acknowledgments

The present work was partially supported by the Multinational Program of Metallurgy sponsored by the Organization of American States (OAS) and the Servicio Naval de Investigación y Desarrollo (SENID) of the Argentine Navy. The authors thank Prof. W.F. Savage for helpful discussions and comments, as well as Eng. L.A. de Vedia and Eng. H. Scagnetti for helpful interactions during different parts of the present work.

References

1. Paton, B., *Electric Slag Welding*. Foring Languages, Publishing House, Moscow.
2. Ellis, D.J., and Gifford, A.F., "Application of Electroslag and Consumable Guide Welding," *Weld. and Met. Fab.*, June 1973, 41 (6), pp. 198-203.
3. Patchett, B.M., Collings, F.W., and Apps, R.L., "Process Parameters and Mechanical Properties of High Speed Consumable Guide Welds," *Weld. and Met. Fab.*, June 1973, 41 (6), pp. 216-224.
4. Eregin, L.P., "Calculating the Penetration in ESW," *Weld Prod.*, July 1970, vol. 17, N°7.
5. Eregin, L.P., "Influence of ESW Setting on the Thermal Cycle in HAZ," *Weld Prod.*, Feb. 1971, Vol. 18, N°2.
6. Prokhorov, N.N., *et al.*, "The Spatial Macrostructure of Weld Metal with Various Forms of Crystallization Front," *Weld Prod.*, 1969, No. 12, pp. 2-7.
7. Granjon, H., et Dadian, M., "Particularitees de la Solidification des Soudures par Fusion," *Soud. Tec. Conn.*, May 1972, Vol. 26 S/6, pp. 181-195.
8. Savage, W.F., Lundin, C.D., and Aronson, R.H., "Weld Metal Solidification Mechanics," *Welding Journal*, 44 (4) April 1965, Res. Suppl., pp. 175-s to 181-s.
9. Lewis, D.M., "Techniques for the Investigation of Thermal Conditions in Continuous Casting," *Journal of the Institute of Metals*, 1953-54, Vol. 82, pp. 395-413.
10. Mitchell, A., "Theory and Practice of Electroslag Remelting," *The Journal of Vacuum Science and Technology*, 1970, vol. 7, N°6.
11. Mitchell, A., *et al.*, "Macrosegregation, Liquid Movement and Heat Flow in ESR Process," *Proceeding of the Fourth International Symposium on ESR processes*, June 1973, Japan.
12. Savage, W.F., Lundin, C.D., and Chase, T.F., "Solidification of Fusion Welds in Face-Centered Cubic Metals," *Welding Journal*, 47 (11) Nov. 1968, Res. Suppl., pp. 522-s to 526-s.
13. Pepe, J.J., and Savage, W.F., "Effects of Constitutional Liquation in 18 Ni Maraging Steel Weldments," *Welding Journal*, 46 (9), Sept. 1967, Res. Suppl., pp. 411-s to 422-s.
14. Biloni, H., Report PMM/R-66 CNEA, Argentina. Report PMM/R-136 CNEA, Argentina.
15. Biloni, H., "The Solidification of Metals," ISI Publication, p. 110, p. 74 (1968).
16. Scagnetti, H.J., de Vedia, L., Solari, M., y Biloni, H., "Soldadura de Grandes Espesores por Electroescoria," Report PMM/C-134, CNEA, Argentina, 1974.
17. Solari, M., y Biloni, H., "Morfología de la Pileta Líquida en Procesos de Refusión y Soldadura por Electroescoria," Report PMM/C-150, CNEA, Argentina 1974.
18. Nippes, E.F., Savage, W.F., and Owczarski, W.A., "The Heat-Affected Zone of Arc-Welded Ductile Iron," *Welding Journal*, 39 (11), Nov. 1960, Res. Suppl., pp. 465-s to 472-s.
19. Hrubec, R.J., "An Investigation of the Effect of Welding Parameters on Segregation and Cracking in HY-80," Thesis, Rensselaer Polytechnic Institute, Troy, N.Y. 1967.
20. Savage, W.F., and Szekeres, S., "Technical Note: A Mechanism for Crack Formation in HY-80 Steel Weldments," *Welding Journal*, 46 (2), Feb. 1967, Res. Suppl., pp. 94-s to 96-s.

"ELECTROSLAG WELDING RESEARCH IN ARGENTINA"

by M.Solari and H. Biloni

ELECTROSLAG WELDING RESEARCH IN ARGENTINA

Mario Solari: Department of Materials, Atomic Energy Commission (CNEA), Buenos Aires, Argentina

Heraldo Biloni: Director of the Multinational Program of Metallurgy OAS-CNEA, Buenos Aires, Argentina

INTRODUCTION

At the Argentine Atomic Energy Commission (CNEA) and under the frame of the Multinational Program of Metallurgy sponsored by the Organization of the American States (OAS) extensive research on metallurgy processes is under way. Special effort is made in connection with Electroslag Welding Technology (ESW) of steel and aluminum. The research approach is to obtain correlations between operational variables, metallurgical structures and mechanical properties. The investigation strategy can be summarized:

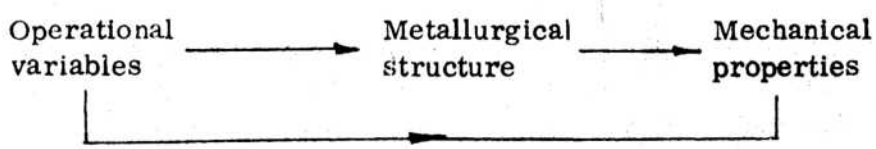

The different stages of the research under way are:

i) Origin and development of the weld structure. The basis of the research are the extensive knowledge developed in solidification and heat transfer at the Solidification and Casting Division of the CNEA, as well as the existing knowledge in solid phase transformations and special metallographic techniques.

ii) Study of the correlations between the weld structure and both the operational variables and mechanical properties.

iii) At the same time is intended to correlate directly the operational variables with the mechanical properties. In these studies the results are used in order to obtain an adequate selection of consumible materials.

The present work intends to give a picture of the results already obtained and published as well as the research in progress.

EXPERIMENTAL TECHNIQUES

Fig. 1 shows the equipment used as well as the device used in order to maintain the plates to be welded in a correct position. A Hobart ES-2 model for ESW was used. This equipment enables the use of either one or two electrodes according to the plate thickness until a limit of 300 mm. The electrode can be used with or without oscillation. When oscillation is used, the frecuency and magnitude of the lateral oscillation can be controlled properly. The energy sources were two Hobart rectifiers RC-1000 of constant potential, having nominal outputs as 85,58 and 35 V.

Structural carbon steel with a maximum of 0.25%C was employed. Plates size were 35x35x5.1 cm. The fluxes were of the commercial type for ESW or those used for submerged arc welding process. Diameter electrode of 0.238 cm and 0.317 cm were employed. Regarding to consumible guides were used commercial type as well as specially designed for the different experiments performed. The variables taken into consideration were: plate thickness, voltage, current intensity, welding feed rate, gap between plates, slag composition and slag level; welding speed, weld geometry, energy input, guide design and guide composition. The structural analysis was performed through standard and special metallographic techniques, sulfur print and X Ray. Mechanical properties were measured through conventional tests.

RESULTS

Stage i) and part of stage ii) were already completed and partially published for low carbon steels. Taking into account the scientific background involved, the results can be summarized.

Different zones can be distinguish in a welded structure; those having as origin the liquid-solid transformation, or primary structure, and those having, as origin, solid phase transformations taking place at the weld or at the HAZ (secondary structure). According to Savage and his school at Rensselaer Plytechnic Institute, the use of special metallography can reveal the following zones in a welded structure:

I) Mixed molten zone

II) Unmixed molten zone

III) Partially melted zone

IV) Heat affected zone (HAZ)

During the research performed in the present Program, these zones were characterized for the ESW process and will be briefly analyzed.

I) Mixed molten zone

The formation of this zone is directly connected with the mechanisms involved in the liquid-solid transformation.

b) Nucleation and growth : In order to solidify, a metal must start from a solid nuclei able to grow under favorable thermodinamic conditions. In the real or industrial world the nucleation is heterogeneous, this is, favoured by the existence of substrates present in the melt. The theory of heterogeneous nucleation affirms that, a good wetting of the substrate by the melt, improves the nucleation. In the specific case of the welding process, this wetting is perfect,

because the substrate is provided by the partial melting of the base metal grains. From there, the solidification of the weld starts. Taking into account that the growing crystals have the same crystallography orientation of the partially melted grains, the process is known as epitaxial growth. However, a preferred growth orientation arises and corresponds to the cellular dendritic substructure developed during the solidification. For the steels, the preferred growth direction is the <100>. As a result, a selection of grains occurs and a growth texture is developed. In general, the weld structure will be columnar, but under determined conditions equiaxed grains could appear stopping the columnar grains. In the present experiments performed with ESW, the structures were always completely columnar.

2) Shape of the pool: The shape of the pool depends upon the welding speed as well as on the heat balance of the system fixed by the heat input and the cooling conditions. If the welding speed is low the pool tends to be plane. On the other hand, if the welding speed increases the pool shape tends to a paraboloid of revolution and as a consequence the pool depth increases. Taking into account that the columnar grains grow, in a direction closely perpendicular to the S-L interface, it is important to know the shape of the pool. In the ESW process this is possible in an indirect way through the sulfur print techniques, were SF_e is added during the process and acts as a tracer. In order to predict the shape of the pool, a simplified heat transfer model was formulated. The model is able to predict, during the steady state condition of the process, the pool shape as a function of the physical properties of the base metal and the operational variables such as welding speed and geometrical configuration of the system. Experimental results obtained show good agreement with the proposed model.

3) Solidification rate: The solidification rate is the projection of the welding speed upon the perpendicular to the S-L interface. As a consequence, it depends upon the welding speed but also on the heat extraction. It starts from zero at the beginning of the epitaxial growth, and reached a maximum at the weld axis.

4) Liquid thermal gradient: Due to the existence of the molten slag, the liquid metal has a certain superheat and, as a consequence a liquid gradient (G) exists. This gradient is a maximum where the distance between the S-L interface and the slag is a minimum. The G value near the interface is very important because it is one of the variables controlling the type of segregation substructures, occurring during the solidification process.

5) Solidification structures and substructures: As has pointed out before the liquid pool shape determines the columnar growth direction as well as the solidification rate and the thermal gradient into the liquid. The columnar grain orientation plays an important role vis a vis with the hot cracking sensitivity. The parameter that takes into account this orientation is the encounter angle of the columnar grains measured on the weld axis. During the experiments an increase of this parameter with the welding speed was observed. On the other hand, the shape factor was measured. This is a parameter that relates the weld with the pool depth. The shape factor is also related to the phenomena involving centerline hot cracking sensitivity. The wire feed speed is an operational variable which has a decisive influence on the encounter angle and the shape factor. This conclusion of the work imposes a maximum limit of the wire feed speed, in order to avoid radial and central hot cracking.

The columnar grains segregation substructure is determined by the S-L

morphology as a function of the relationship existing between the liquid thermal gradient, G, and the solidification rate (V). This corresponds to the Constitutional Supercooling concept introduced by Chalmers and his school. For a high G/V relationship the S-L interface will be plane; this occurs at the beginning of the epitaxial growth. Quite rapidly the S-L interface becomes unestable and in practice reaches the condition of a cooperative growth of dendrites known as cellular dendrites.

Microsegregation -short range segregation- is a consequence of the solute redistribution during solidification.

6) "Mushy"zone: The solidification process in an alloy proceeds in a temperature range between the liquidus and solidus lines of the equilibrium diagram. As a consequence, a coexistence of liquid and solid between both isothermes exists. This is the "mushy zone". The width of this zone and its displacement rate, determine the time of the completion of the liquid-solid transformation at each point of the system. This parameter is known as "local solidification time", it can be calculated and depends on the conditions imposed to the solidification process.

7) Solidification microstructure: The mushy zone characteristics, together with the cellular dendritic substructure, produced by the Constitutional Supercooling conditions, existing during the columnar growth, determine structural elements of different type: i) microsegregation as a consequence of the cellular dendritic growth, where the dendritic arm space is a direct function of the solidification local time. ii) Non metallic inclusions at the interdendritic spaces. iii) Microporosity. In the actual weld thin structural elements, appears in a proportion related with operative variables. All these structural elements affect directly the mechanical properties. On the other hand the solute enriched liquid flowing into the cellular dendritic channels, can produce macrosegregation, this is a long range segregation

one of the causes of hot cracking during the ESW process at high welding speeds.

8) Liquid flow into the pool: The solidification parameters mentioned above can be affected by the liquid stirring due to different causes: thermal convection or forced convection by mechanical or electromagnetic devices. The possible effects must be taken into account, in order to control the structure of the weld.

9) Banding: During the welding process occurs a periodic fluctuation of the solidification rate and the thermal gradient. As a consequence a localized variation of composition appears, named banding. When a suitable metallographic etching is used the local solute variation can be detected and the pool shape is revealed.

10) Phases: When steel is welded the grains begin to solidify with a structure corresponding either to ferrite ( ) or austenite ( ) depending on the carbon alloy content and cooling rate. During the cooling until room temperature that phase suffers solid phase transformation. The unhomogeneity composition, result of the solidification substructure has as a consequence different solid phase transformations at different points of the weld. That differences are functions of the local carbon and other alloy elements content. Different types of inclusions appear related with the original position of the primary interdendritic spaces.

II) Unmixed molten zone

The metal transfer, from the base metal to the liquid pool, is through a doplet mechanism and a sliding of molten base metal. The second mechanism, forms unmixed projections of melted base metal into the weld. In the ESW process this effect can be metallographically detected through proper etching techniques.

III) Partially melted zone

During the welding process, the base metal near the fusion line is submitted to a thermal cycle and, as a consequence, inclusions of low melting point, as well as segregates regions, due to partition coefficients less than 1, can be melted. From the technical point of view this phenomenon is very important because those regions, when solidified, and contracted, during the subsequent cooling are, in general, source of microcracks.

Secondary structure: As has been mentioned before, the subsequent cooling to the liquid-solid transformation provoque the formation of the so called secondary structure. In the case of the steels, according to the cooling cycle, the fases or formed at high temperature will be transformed in the structures emerging from the TTT (Time, Temperature, Transformation) diagram corresponding to the welded steel, this is ferrite, bainite, etc. When ferrite is formed its morphology depends upon the cooling conditions, as well as the chemical composition of the steel. The phase transformation begins with the ferrite nucleation at preferential places, as grain boundaries and segregated areas. The influence of the primary structure on this transformation is still not completely clear and in the research under progress the relationship existing between the solidification substructure and the resultant secondary structure is investigated. The secondary macrostructure has the same aspect as the solidification macrostructure, but instead of austenite, or delta grains, numerous and small ferrita grains appear that coexist with perlite or other solid phase transformations products. At present, in the ESW process experiments under way, the relationship between the segregated areas of the primary substructure and the ferrite nucleation has been determined, but the mechanism acting during the solid phase transformation is still under research. In reference with another

structural elements that were formed during the weld solidification, as inclusions, pores, macrosegregation, etc. are not affected by the solid phase transformation and, as a consequence, are presents in the final structure.

IV) Heat affected zone (HAZ)

The metal near the weld is submitted to a heterogeneous thermal cycle producing different solid phase transformations as a function of temperature and time. The result, is different structures, characterized by different grain size. Near the fusion line the grain size is larger and it is convenient to obtain the thinnest HAZ possible. This can be managed decreasing the energy input through either a lower Voltage or an increase of the welding speed. This procedure is more convenient and is obtained when the gap between plates to be welded is disminished.

In summary, the weld structure is composed by different elements having, as origin, the liquid-solid transformations and solid phase transformations. The results are columnar grains to be joined at the weld axis. The interior of these grains presents an elevated chemical heterogenity associated with inclusions and microporosities.

Finally, the resultant structure of a weld, can be changed as a function of the operating variables. As an example, increasing the "energy input", the dendritic space increases, as well as the size of the inclusions. On the other hand for a given voltage an increase of the wire feed rate has, as a consequence:

1. The penetration remains approximately constant
2. The pool depth increases
3. The shape factor decreases
4. The encounter angle increases

5. The shape of the pool becomes approximately parboloid of revolution.

Fig. 2 corresponds to the structural results obtained, meanwhile Fig. 3 shows the sulfur print of the pool.

MECHANICAL PROPERTIES VERSUS WELDING STRUCTURES

This part of the work, under progress, corresponds to points ii) and iii) and takes into account the relationship between the welded structures and the mechanical properties, but at the same time, the direct way mentioned at the Introduction. In the first approach, low carbon steel plates of 5.8 cm thickness are used with different consumables and operational variables. The welded structures are submitted to different tests as traction, bending and impact, as well as inspection through metallography and non destructive tests. At present, the ESW process used is the high speed type where the gap between plates to be welded is 16-18 mm, instead of the conventional 25.4 mm. With this method the welding speed is larger than 4 m/h and the HAZ is drastically reduced. Fig. 4 compares the conventional results with those obtained at high welding speed. In order to obtain this type of weld, a specially designed consumable guide is used, shown at Fig. 5. The analysis of the structures obtained, shows that the speed of the process has a limit, from where radial cracking appears, associated with macrosegregation of alloy elements.

The second approach corresponds to the direct correlation between consumable and mechanical properties, obtained through different mechanical tests. In this case wire, with different chemical composition and different slags are used. This research approach permits an adecquate optimization of the operational variables, consumable selection and qualification of the welding procedure, but the reason of the results obtained is not cleared up. From the authors point of view, both

approaches to the research are valid, but the extrapolation of the results obtained, only is possible through a complete study envolving operational variables, structural analysis and mechanical properties.

ELECTROSLAG WELDING OF ALUMINUM AND ITS ALLOYS

Every day the thickness of structural aluminum parts to be welded increases. As an example can be quoted the busbars in aluminum plants, or structural parts of liquid petroleoum gas containers. A comparative study of the possible methods to be used shows that the MIG process is useful until 45 mm thickness, the electro-gas process in a range between 30 and 70 mm, while the electrobeam can be used between 30 and 120 mm. The ESW process can be used for thickness larger than 40 mm and from the economic point of view, presents the best conditions. However, the ESW method in aluminum alloys is not popular, probably because the complexity inherent to the aluminum welding is connected with very little scientific-technical information, related to this method.

The ESW research program under way, considers the ESW of aluminum and its alloys. It should be considered that for a given aluminum to be welded, the energy necessary for the melting is less than for a similar steel volume, but the high thermal conductivity of the aluminum imposes a high heat input, in order to obtain a proper penetration. The existence of a Al_2O_3 film difficult to be removed, even when the base metal has been melted, is another important factor. At present the different research areas are:

1) Slag selection

2) Consumable guides design and selection of the proper wires to be used

3) Design of the refrigerant devices of the equipment, considering the high thermal conductivity and specific heat of the aluminum

4) Gas extraction system, design, in order to protect the equipment and the operator from toxic products

SUMMARY

Under the frame of the Multinational Program of Metallurgy OAS-CNEA, a research of the ESW of steels and aluminum alloys is under way at the Atomic Energy Commission of Argentina. The strategy research is to know the origin and development of the weld structures obtained and their relationship with the resultant mechanical properties. This purpose an interrelation among operational variables, structures and mechanical properties. This optic permits to obtain general knowledge on the welding metallurgy, able to be extrapolated to other process and materials. On the other hand, the direct way, where the consumables and operational variables are related with the mechanical properties of the weld, withouth considering the structure, seems to be correct for an adecquate selection of consumables and procedure qualification, but is limited for a complete understanding of the welding processes. The use of a high speed welding for steels reduces the HAZ and the metal to be deposited for a given plate thickness considerably. With reference to the application of the ESW in aluminum alloys, the preliminary results obtained can be considered positive.

CAPTIONS

Fig. 1 Equipment used in the ESW research

Fig. 2 Structural results obtained in ESW of low carbon steels

Fig. 3 Sulfur print showing the poool shape

Fig. 4 Comparision between weld structures for conventional and high speeds methods

Fig. 5 Guide consumable design for high speed ESW

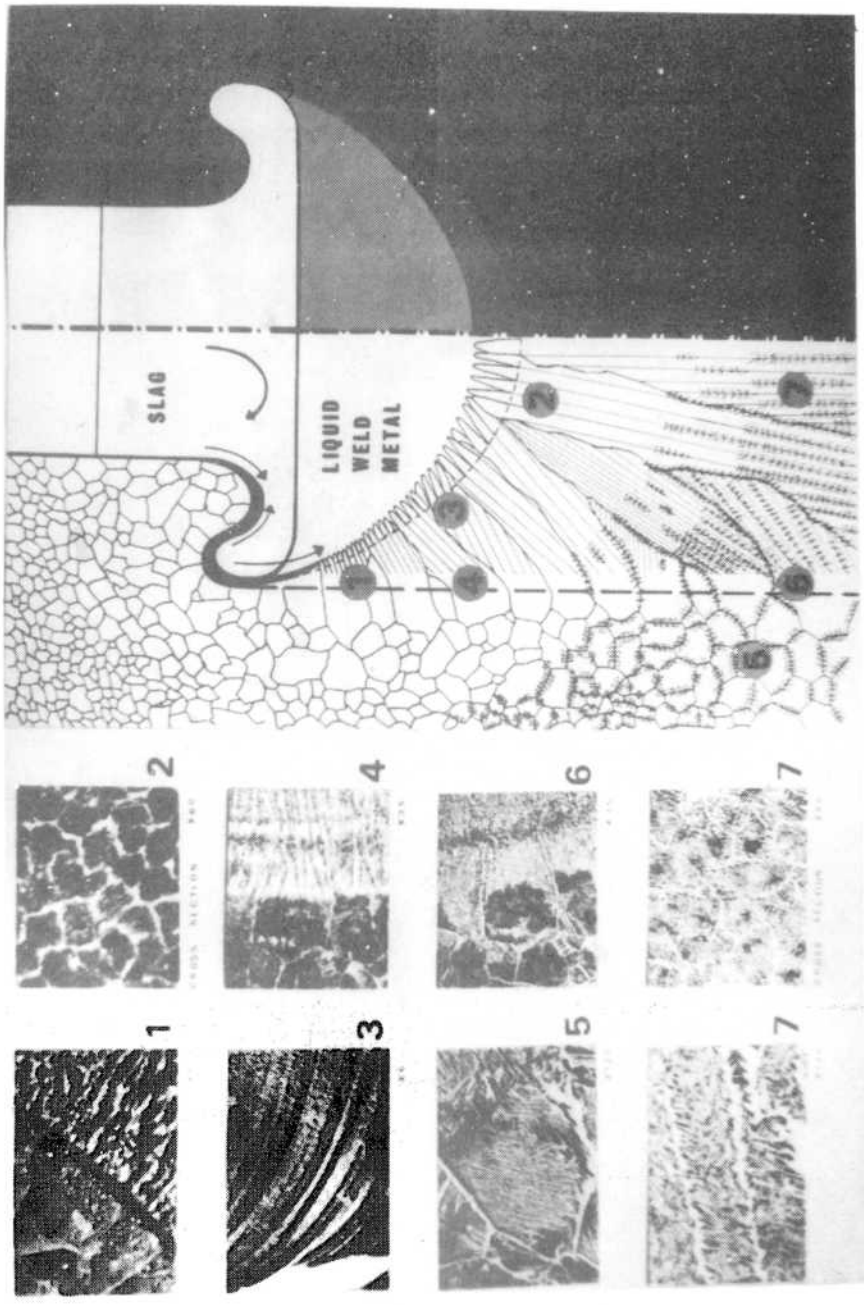

Fig. 2

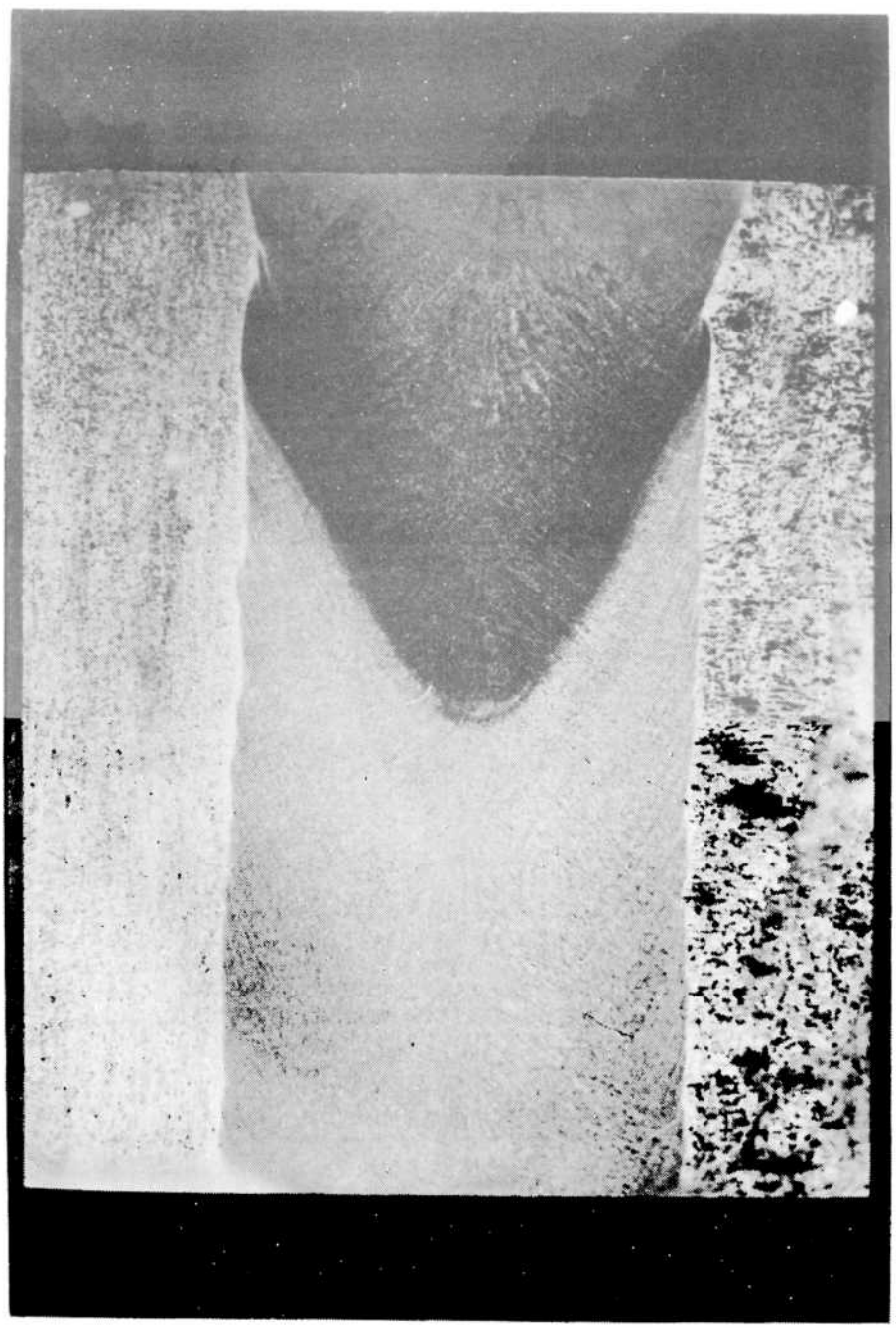

Fig. 3

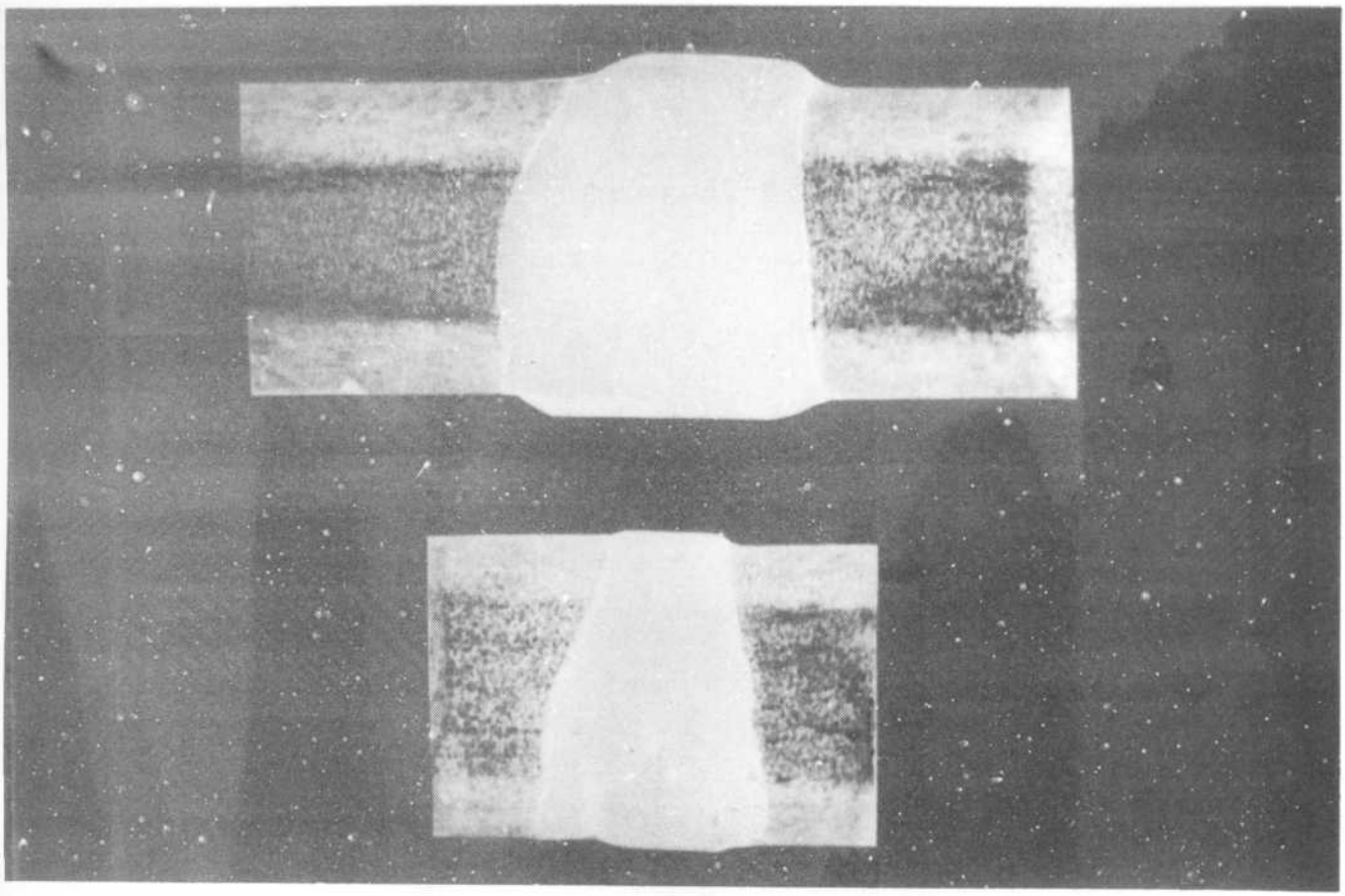

Fig. 4

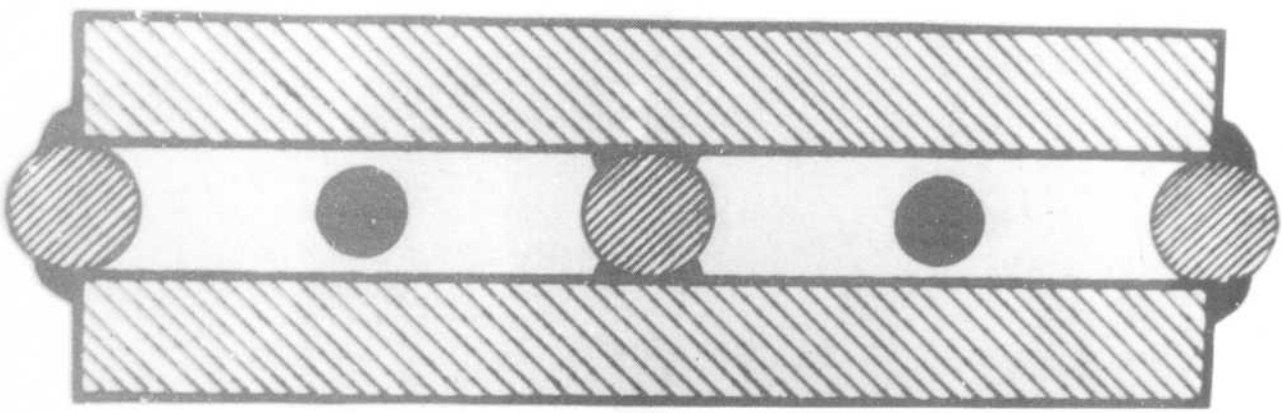

"FUSION WELDING MACROSTRUCTURES"

by T.E.Pérez, M. Solari and H. Biloni

ORIGIN AND DEVELOPMENT OF FUSION WELDING MACROSTRUCTURES

T. Pérez, M.J.Solari and H.Biloni

I) INTRODUCTION

The weld metal structure is a result of complex transformations and interactions, starting with metal-gas and metal-flux reactions in the liquid state. The primary structure is obtained through the liquid-solid transformation, which generally, follows certain laws, quite well understood, at present, after 30 years of research in controlled solidification

An actual structure (eventually secondary) is obtained as a consequence of thermomechanical transformations occurring during the subsequent cooling till room temperature. The final structure is composed /by elements/ such as different phases, physical and chemical heterogeneities, which interact with the constraints imposed by the weld geometry. As in all metal structures the analysis can be done in three stages: i) Macroscopic scale: that characterizes the shape, size, distribution and orientation of the grains. This is known as "macrostructure"; ii) microscopic scale: microsegregation, inclusions, microporosity, etc.: iii) crystallographic and atomic level, mostly related with crystal lattice defects.

Taking into consideration that the classification of the primary and secondary structures is still not clear the present work will attempt to clarify and unify that classification. While some authors refer to primary structure, others consider the secondary structure. Savage (1) describes several types of columnar structures in relation with the weld pool morphology, adding an axial grain structure. Paton (2), working with electroslag process in steels describes four types of structures: fine columnar grains, coarse columnar grains, "mixed grains" and central equiaxed grains. Kerr (3), in agreement with Russian authors (2) describes the following structures in TIG steel welds: i) axial; ii) stray; iii) columnar; iv) competitive columnar; v) equiaxed and vi) partially equiaxed . On the other hand, Edvarsson (4) reported axial growth in submerged arc processes controlled by groove angle variations. Kato and Matsuda (5) described several types of macrostructures in aluminum alloys, analysing the welding speed and the alloy composition influence. Finally Nakada et al (6) described another structure already discussed in aluminum alloy castings: the feathery crystals. The research strategy to be used is the same applied by Biloni and coworkers in casting research (7), this is, the relationship existing between microsegregation substructures and the resultant macrostructure. With this aim electroslag and submerged arc welding

experiments have been performed, in steels as well as the analysis of aluminum welding alloys using automatic tungsten arc process. The results obtained will be compared and discussed with those previously existing in the literature, in an effort to establish in a rational way the origin and development of the different fusion welding structures.

II) EXPERIMENTAL

1.- Equipment

i) Electroslag and submerged arc processes: Two constant potencial D.C. electrical power suplies were used. The maximun intensity was 1000 Amp each one.

ii) Automatic TIG process: A device able to operate either in direct or alterning current was used , with H.F. in order to start the arc.

2.- Materials

Table I gives details on the chemical composition of the base and filler metals as well as on the geometry of the weld, consumable guides and fluxes used.

3.- Welding procedure

i) Electroslag process: A butt joint with a gap of 2.5. cm and consumable guides without oscillation were used. In order to maintain constant the slag depth , flux was added during the operation. The welding voltage was 40 Volts and the electrode speed rate ranged between 5 and 19 cm/seg. Reverse polarity was used. The welding intensity varied between 400 and 1000 Amp.

ii) Submerged arc process: Bead on plate weldments were prepared using reverse polarity. The welding parameters varied in the following ranges: Current 400 to 600 Amp; Voltage 22 to 34 V; welding speed 18 to 98 cm/min.

iii) Automatig TIG Process: Alterning current, tungsten electrode (0.8% Zr) and argon shielding gas were used in order to produce bead on plate weldments. The weldment parameters varied as follows: Current 60 to 150 Amp; Voltage 10 to 20 V; welding speed 20 to 100 cm/min.

4.- Metallographic techniques

i) Steels

a) Nital 10% in order to reveal the macrostructure

b) Nital 1% to reveal the microstructure.

c) $FeCl_3$: 40 gr.; $CuCl_2$: 3 gr; HCL: 40 cm^3; ethyl alcohol: 500 cm^3

ii) Aluminum

a) Electropolishing followed by etching with: HNO_3: 47 cm^3; HF : 3 cm^3; H_2O : 50 cm^3. This etchant reveals the microstructure

b) Mechanical polishing until 1 micron alumina, followed by etching with: HCl: 50 cm^3; HNO_3: 47 cm^3; HF: 3 cm^3. This etchant reveals the macrostructure

5.- "Encounter angle measurements"

The encouter angle in electroslag and submerged arc weldments is determined by the impingement between the columnar grains and the central line. (Fig.1)

6.- Complementary experiments

In order to elucidate the structure called "partially equiaxed" (3) , casting experiments in laboratory scale were performed. 6063 alloy ingots were casted in copper molds of 6 cm diameter and 10 cm high. The ingot structure was observed as cast and after subsquent electrolytical polishing,

III.- EXPERIMENTAL RESULTS

1.- Electroslag process

Table II summarizes the welding conditions as well as the measured encounter angle.

a) The macrostructure obtained in steels type A is constituted only by columnar grains. Originated in the base metal, they grow towards the center of the bead with an encounter angle that increases with the electrode feed rate. Fig.2 shows the macrostructure after etching with Nital 10% and Fig.3 corresponds to the secondary microstructure produced during the solid state transformations. The analysis of the segregation substructures through suitable etchants show that when the feed rate is high the grains define an encounter line at the bead axis (Fig.4). For lower feed rates one or more axial grains are detected stopping the columnar growth (Fig. 5).

b) In steel type B, with higher amount of carbon the secondary structure is formed by coarse columnar grains

growing epitaxially from the parent metal. This coarse grains are followed by fine columnar grains covering the central zone of the weld , (Fig. 6).

2.- Submerged arc

Table III shows the welding conditions. In this case for a given welding speed the encounter angle varies essentially with the welding current. For high welding intensities two angle were measured. The greatest corresponds to the columnar grains that grow from the base metal. The smallest is measured from the point where the columnar grains modify their direction. Taking into consideration that a proper measure of the encounter angle must be done in three dimensions, it may be possible that the anomalies observed in the tendency variation, as are shown in Table III, are due to studying only the metallographic plane. Fig. 7, corresponding to a transversal section, shows the mentioned encounter angles. Eventually some axial grains could appear intercepting the columnar grain growth.

3.- Automatic TIG process

Fig. 8 shows the longitudinal cross section corresponding to a weldment performed in Aluminum 99,5A stray structure is noticeable, as well as axial grains stopping the columnar growth. This type of structure has been also observed in Aluminum alloy 6063 .Under some welding conditions an equiaxial central structure was observed in the same alloy , Fig. 9.On the other hand Fig. 10 corresponds to a typical feathery crystal structure obtained in a 5086 Aluminum sheet.

4.- Additional experiments

In the surface of 6063 aluminum ingots the so called "meniscus marks" (8) were analyzed.The as cast surfaces presents a superficial structure with the appearence of small equiaxed or multiplied grains. Fig. 11 (a-d) shows the microstructure as cast and after subsequent electrolytical polishing. It is quite clear that the structure is confined to a thin superficial film of the ingot.

IV) DISCUSSION AND CONCLUSIONS:

In the attempt of classifying fusion weld macrostructures we considered worthwhile to correlate their origin not only with the phase transformation ocurring during the process but also with the mechanism of solidification . The results obtained by Kerr and other authors (5,9) are also taken

into consideration. The following concepts are those considered basical for the discussion.

1.- Liquid - Solid transformations

i) Epitaxial and competitive growth of the columnar structure from the base metal (9)

ii) Interface instablity as a result of the amount of Constitutional Supercooling (10). A sequence of different segregation substructures: cellular, cellular dendritic, dendritic and superdendritic, are obtained at increasing supercooling.

iii) Crystal multiplication (11) and nucleation on the free surface (12).

iv) Peritectic reactions influencing the subsequent solid phase transformations in steels.

2.- Solid phase transformations

After welding operation on steels, and during the subsequent cooling, new phases are nucleated in the solid state. The structures obtained are, in general, related to the solidification substructures.
Fig.12 shows schematically the different types of macrostructures present in fusion welds, together with the mechanisms involved in their origin and development.
Based on the previous mechamisms those structures can be explained as follows:

Type N° 1: Columnar structure: the columnar grains impinge at the bead axis determining a defined encounter central line. The grains are formed epitaxially and due to the competitive growth only those with an easy growth direction, nearly coincident with the heat extraction, reach the center.
This structure is associated with tear shaped weld pools, that is to say, with high welding speeds.
The interface instability and, therefore, the resulting substructure are function of: the growth speed, the thermal gradient and the metal composition.
In general, a cellular dendritic substructure is obtained with commercial alloys.

Type N° 2: Competitive columnar structure: in this case the central line is irregular, as shown in Fig. 12

This structure was found in steels containing 0,08 % C and at welding speed above 30 cm/min.(3).
The transition from structure type 1 to type 2 is gradual; and sometimes, they coexist.
When the composition and the welding speed exceed determined values a preferential growth of certain dendrites is observed. As the thermal gradient tends to zero, the structure can be supposed to be formed by superdendrites (13), this mechanism was observed in castings.

Type N° 3: in this case the columnar grains do not form a defined center line.
This structure appears when th welding speed is low and consequently, the weld pool is elliptical.
The grains grow normally to the liquid-solid interface following the maximum thermal gradient, as it changes. Fig.2 shows this structure in an electroslag weldment.

Type N° 4: Stray structure: the characteristic of this structure is that many grains,which grow epitaxially from the base metal, are stopped by nuclei that float in the liquid.
Several authors (10,11,15) have established the existence of the so called "initial zones" , they are originated by crystals that grow free in the liquid; the initial zones segregation substructures presents a coarse region, followed by a celluar dendritic substructure . During the free growth the heat is transfered from the solid towards the liquid. When the columnar grains,which grow from the base metal,touch a nucleus , heat is extracted through the solid, producing a dendritic morfology.
As a function of the nuclei density , the final structure would be equiaxed or stray; in this case the nuclei generate new columnar grains.
Three possible mechanisms can explain the origin of initial zones. These mechanisms operate,to various degrees, in the cast ingots equiaxed zone formation ; their application in welding are analyzed as follows:

i.- Southin mechanisms (12): nucleation events are produced at the free surface, and the nuclei are showered down into the liquid. In arc welding this mechanisms is very improbable because the heat source would melt the nuclei; in electroslag welding this mechanisms can not operate due to the weld geometry.

ii.- Winegard and Chalmers (16) propose a mechanism of heterogeneous nucleation in the melt. It is also scarcely probable in welding due to the presence of a positive thermal gradient in the liquid.

iii.- Jackson et al (11) and O'Hara and Tiller (17,18) proposed the crystal-multiplication mechanism. In it branches of the columnar structure are broken due to the heat flow and thermal convection.
The presence of solid fragments trapped in the columnar front of a weld is promoted by conditions which enhance constitutional supercooling and dendrite remelting. A prove to this theory is that larger fragments showing evidence of free dendritic growth are observed at higher solute contents (15). Kerr (3), also, observed that an increase in solute, promotes grain multiplication.

A longitudinal cross section of an aluminum weldment, with stray structure, is shown in Fig. 8 b.

Type N° 5: Axial structure: several grains grow following the bead axis direction stopping the columnar growth. In this case, the maximun thermal gradient direction coincides with the weld axis. That is why the columnar grains, that grow from the base metal, have a non favorable direction and the growth of a few grains parallel to the axis, is easier.
This structure is shown in Fig.8 a
Edvardsson (19) studied the growth direction in a transversal cross section and defined an encounter angle; it is function of the welding current intensity, the voltage and the welding speed. The crystals can grow diverging from a point at the botton of the bead or develop as parallel plates.
It is also possible that some of the grains , which were growing epitaxially form the base metal, change their direction and continue growing parallel to the center line axis; in this case the transversal section looks like fig.
Cracks frecuently appear in the grain boundaries of the axial grains (4, 20) , as it is shown in Fig. 8 a in aluminum weldment.
These structure also appears in electroslag and submerged arc welding (Figs. 5 and 7b).

Type N° 6: Equiaxed structure was found in aluminum alloys, specially as the solute content increased . Fig. 9 shows an equiaxed structure obtained in aluminum 6063.
Kerr (3) concluded that the percentage of equiaxed region, in steel welds, decreases as the carbon content increases; this observation suggested that constitutional undercooling was not responsible for equiaxed grain formation. He considers the heterogeneous nucleation mechanism, to be the source of equiaxed grains near the center for a weld; on the other hand Arata (21) is

in agreement with the S.C.theory Kerr (3) presents another structure that he calls "partially equiaxed" . Equiaxed grains can be noted superficially in a longitudinal cross sections, but they can not be observed in a transversal cross section.
The additional experiments carried out during the presents work, sugget that the origin of this structure is similar to that of the"meniscos marks" Fig. 13 shows a scheme of the proposed mechanism for both cases. During solidification, a contraction skrinkage is formed and if the liquid feed is deficient, the dendritic morphology is shown plainly in the surface, and the superficial segregation is the result of solute liquid enrichnent.

Type N° 7: Feathery crystal structure: was found in aluminum weldments and continuous casting . This structure is formed by plates, nearly parallel,forming a conical or pyramidal colony, (22) Their thickness is about 100 μ and their length reach some centimeters. Roman, Solari and Biloni (22) analyzed the growing morphology,origin and easier growing directions of this structure in DC casting, this basic analysis is applicable in weldments.

Type N° 8: Structure with coarse and fine grains:Paton identified this structure many years ago (2), but its origin is not yet completely clear.
The appearence of coarse and fine grains is due to the preferential precipitation of poligonal ferrite in certain places. Near the fusion line,the precipitation takes place in the primary grain boundaries (austenitic phase), so that coarse grains are delineated. In the central zone, the ferrite nucleates in the microsegregated regions that appeared during solidification process. One of the proposed mechanisms which explain this structure suggets that the interdendritic segregation in the central zone reaches values which locally modify the curves, and therefore , the feritic precipitation is also influenced.
Another mechanism connected this structure with the solidification sequence and the peritectic reaction ($L + \delta \rightarrow \gamma$) According to this model (23) , coarse grains are obtained when the liquid solidifies as γ phase. On the other hand when the liquid becomes δ ferrite, first, and then, during the peritectic reaction austenite of a different size is produced; finally the descomposition originates a fine ferritie pearlitie structure.
The solidification sequence depends on the cooling rate. In the central region, as the cooling rate is lower equilibrium diagram, and δ ferrite is formed.
Near the fusion line the heat extraction is greater and the metastable reaction $L \rightarrow \gamma$ takes place, this reaction is represented in the Fc.C diagram, continuing the solidus-liquidus lines.

Type N° 9: Structure with coarse and fine columnar grains and an equiaxed central zone: Paton (2) has found this structure in

electroslag weldments of steels with carbon contents over 0,35% and high welding currents. The width of the equiaxed zone varied in the range of 0,4 to 0,8 cm.
In no case, independently of the steel used were equiaxed grain structure found during the present work.

Conclussions

The fusion welding macrostructures can be sketched as Fig. shows, and their origins explained, as followed:

Type N° 1: Columnar structure: origin epitaxial and competitive growth; interface instability.

Type N° 2: Competitive columnar structure: origin epitaxial and competitive growth; interface inestability.

Type N° 3: Origin epitaxial and competitive growth.

Type N° 4: Stray structure: origin epitaxial and competitive growth, crystal multiplication.

Type N° 5: Axial structure: origin epitaxial and competitive growth.

Type N° 6: Equiaxed structure origin epitaxial and competitive growth, heterogeneous nucleation.

Type N° 7: Feathery crystal structure: origin epitaxial and competitive growth; interface instability : constitutional supercooling.

Type N° 8: Structure with coarse and fine columnar grains : origin epitaxial and competitive growth; peritectic reaction; ferrite nucleation and growth.

Type N° 9: Structure with coarse fine columnar grains and an equiaxed central zone.
Origin: epitaxial and competitive growth; interface instability: heterogeneous nucleation or crystal multiplication; peritectic reaction; ferritic nucleation and growth.

Table I

Base metals, electrodes, consumable guides and fluxes compositions

PROCESS	
ELECTROSLAG	Base metal Composition (%) Steel A: C: 0.07 Mn: 0.48 Si: 0.05 S: 0.039 P:0.012 Steel B: C:0.19 Mn: 0.65 Si: 0.12 S: 0.018 P:0.011 Dimensions 35 x 35 x 5.1 cm Consumable guide Composition (%) C:0.1? Mn: 0.65 Si:0.12 S:0.018 P:0.011 Electrode Composition (%) C:0.0 Mn:1.15 Si:0.54 S:0.016 P:0.020 Diameter 0.238 cm 3/32") Flux (%) SiO_2:36.29;MnO_2;27.37;CaO:16.82;Al_2O_3:8.72 MgO:2.67;TiO_2:2.53;Fe_2O_3:1.27;Na_2O:0.93; K_2O:0.72
SUBMERGED ARC	Base Metal Composition (%) C:0.1 Mn:0.75 Si:0.07 Al:0.05 Electrode Composition (%) C:0.11 Mn:1.06 Si:0.11 S:0.02 P:0.021 Diameter 0.325 cm Flux (%) MnO:30;SiO_2:40;Al_2O_3:15;Fe_2O_3:1;BaO:2; MgO+CaO:5;F_2Ca:5;TiO_2:2;K_2O+Na_2O:1 Flux basicity 0.52

AUTOMATIC TIG	Base metals: a - Aluminum alloys - 99,5 Al 99,5 Fe 0,27 Si 0,12 -6063 alloy Fe 0,18 Mg 0,52 Si 0,42 -5086 alloy Fe 0,39 Mg 3,47 Si 0,11 Cu 0,045 Mn 0,32 Cr 0,19 Thickness: 0,1 - 0,2 - 0,25 - 0,3 cm b - Steel C 0,06 Si 0,02 Mn 0,32 Thickness: 0,15 cm

Table II

Welding variables and Experimental Results

Weld Code	Steel	Electrode feed rate (cm/seg)	Current (Amp)	Voltage (V)	Travel speed (cm/min)	Encounter angle(°)
1	A	7.0	450	40	1.22	45
2	A	7.0	450	40	1.22	35
3	A	7.0	450	40	1.22	58
4	A	11.0	600	40	1.91	-
5	A	13.5	700	40	2.34	80
6	A	13.0	700	40	2.34	83
7	A	19.0	900	40	3.3	110
8	A	19.0	900	40	3.3	92
9	A	19.0	900	40	3.3	115
10	A	19.0	900	40	3.3	120
11	B	10.0	600	40	1.85	22

Table III

Submerged arc Welding encounter angles (V: 30 volts).

Travel speed (cm/min) / Current (Amp)	18.78	26.78	50	65.1	97.72
400	67.38	56.28	34.4	22.62	17.06
500	97	71.56	75.54	57.62	83.96
600	82.92	118.08	115.66	97.24	88.48;
650	169 (76.16)	168.58 (76.3)	156.58 124.7	180 (116)	167.76 (80.2)

REFRENCES

1.- Savage , Lundin and Hrubec, Welding Journal, 47 (9), Sept, 1968. Researcl. Suppl, pp 420 (S) to 425 (S)

2.- Paton, "Electric slag welding "Foring Languages Publishing House, Moscow.

3.- Ganaha and Kerr, Metals Technology, 5, (2), Febr.1978, 62 to 69.

4.- Backerud and Edvardsson, Scand. J. Metallurgy, 5,1976, 92 to 96.

5.- Kato, Matsuda and Senda, Trans. JWS V.3, N°1, Sept.1972 69 to 76.

6.- Nakagawa, Katoh , Matsuda and Senda, Trans JWS, V 3, N°2, Sept 1972, 74 to 63.

7.- Biloni Proceeding of Solidification and Casting Conference, Brigthton, 196,.

8.- Morales, Glicksnan and Biloni, Sheffield Intern.Conference on Solidification and Casting, 1977.

9.- Savage, Lundin and Aronson, Welding Journal, 44(4)1965. Research Suppl.175(s) to 181 (s).

10.- Chalmers, "Principles of Solidification" John Wiley and NY, 1964.

11.- Jackson, Hunt, Uhlmann and Senard III, "The equiaxed zone in casting".

12.- Southin, Trans. Met. Soc AIME, V.239,1967, p220.

13.- Cole and Bolling, Ford Motor Co. Publication Preprint, March, 15, 1967.

14.- Biloni: "The Solidification of Metals" ISI N°110 , London, 1968.

15.- Davies and Garland, Int. Met. Rev, 1975, V.20, Review196,83.

16.- Winegard and Chalmers.Trans. Amer.Soc.Metals, 46,1214 (1954).

17.- S.O'Hara and Tiller, Report N°8 AF OSR 731.65 Part I, Dept. of Materials Sci, Standfort Univ. Standfort, California.

...///

18.- Idem 17 Part II.

19.- Bäckerud and Edvardson , Scand. J. Met, 1975 .267 to 272.

20.- Saggese, Solari and Biloni to be published .

21.- Arata, Trans. Japan Weld, Res. Fund.1974 ,3,89.

22.- Roman, Solari and Biloni, PMM/I 228, 1977

23.- Solari and Biloni, Proceedings First Argentine Welding Congress, Bs. As. , 1978.

Figures

Fig.1: Columnar growth encounter angle (scheme).

Fig.2: Longitudinal cross section macrostructure (electroslag welding; steel A).

Fig.3: Secondary microstructure of weld metal (see Fig. 2)(120 x)

Fig.4: Longitudinal cross section structure (high welding speed).

Fig.5: Longitudinal cross section structure (low welding speed).

Fig.6: Coarse and fine grain structure (electroslag welding; steel B).

Fig.7: a- Submerged arc welding macrostructure (transversal cross section) (4,7 x)

b- Segregation substructure of the weld in Fig.7a.

Fig.8: a- Automatic TIG welding macrostructure (Al 99,5) (6,2 x).

b- Automatic TIG welding macrostructure (6063 alloy) (6,6, x).

Fig.9: Automatic TIG welding macrostructure (6063 alloy) (5,7 x).

Fig.10: Automatic TIG welding macrostructure (5086 alloy) (10,7 x).

Fig.11: a) "Meniscus" structure, as cast. SEM. micrograph (240 x).

b) "Meniscus" structure Electrolitically polished.

Fig.12: Diferent types structure scheme.

Fig.13: Mechamism of parcially equiaxed structure origin.

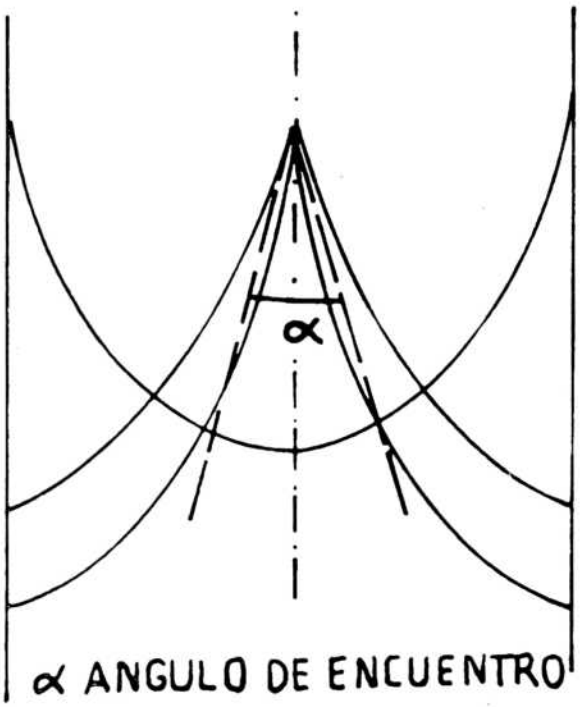

Fig. 1

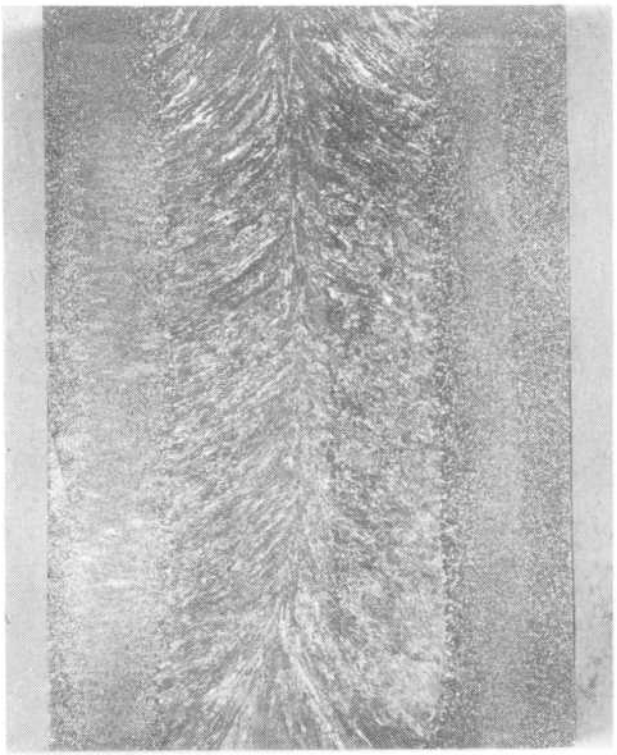

Fig. 2

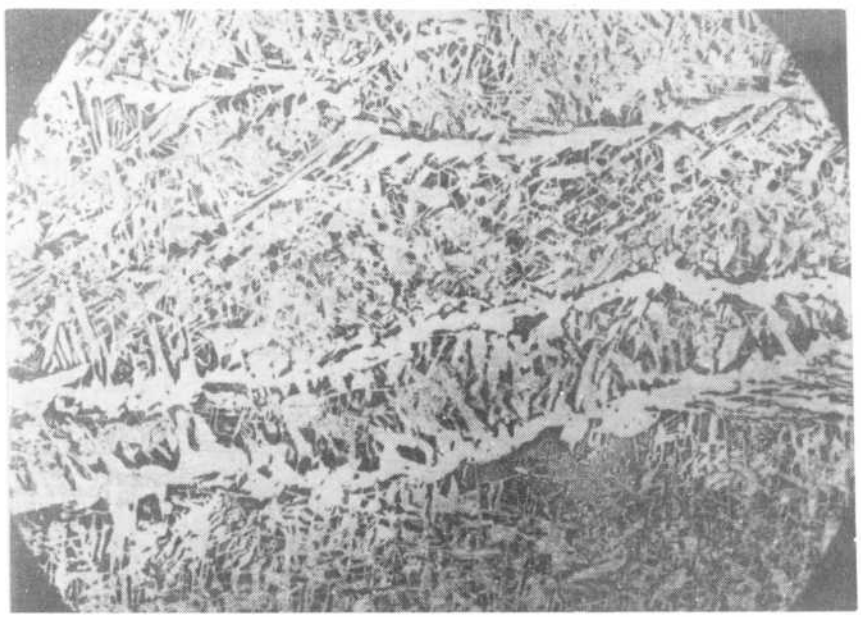

Fig . 3

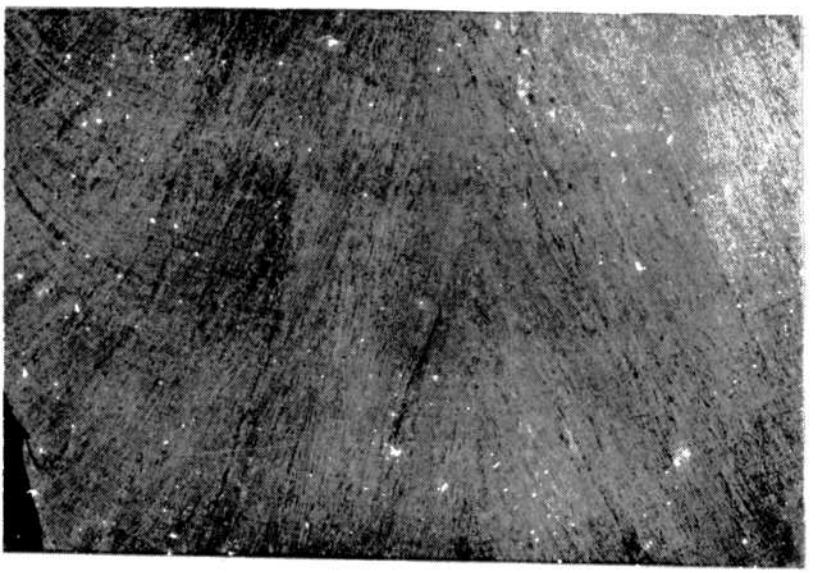

Fig.4

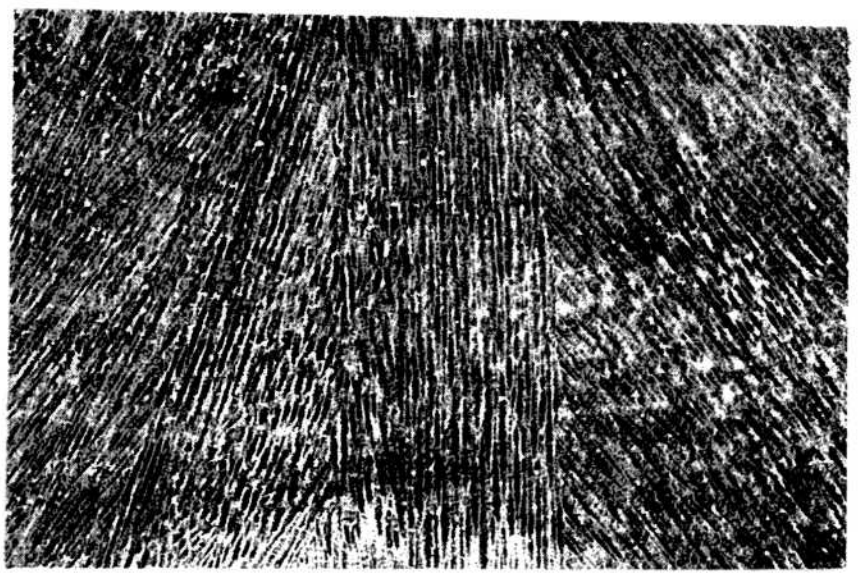

Fig.5

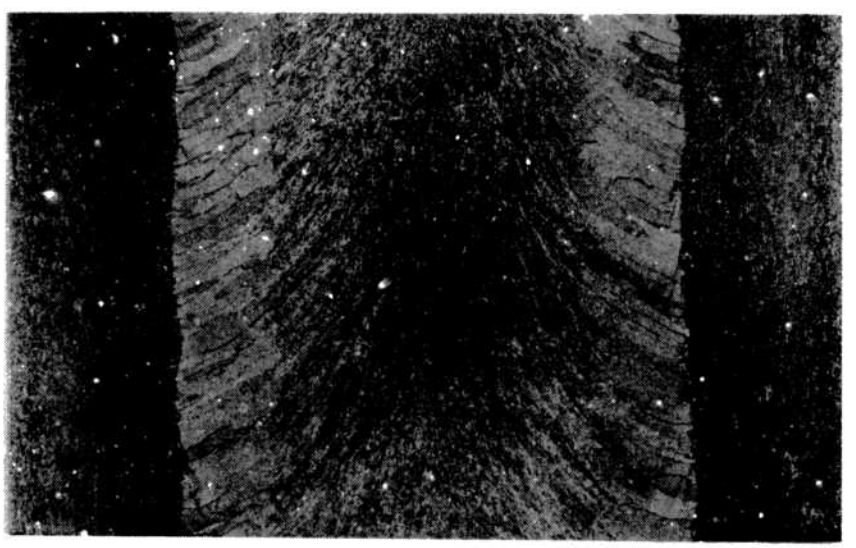

Fig.6

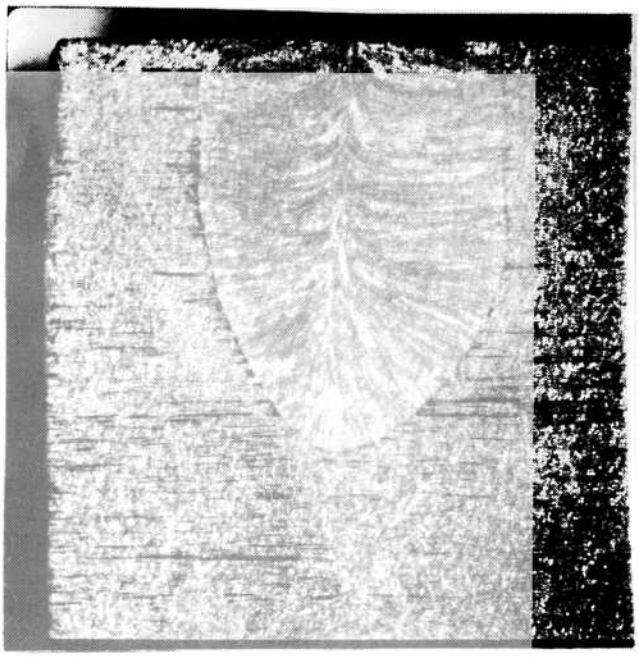

Fig. 7 a

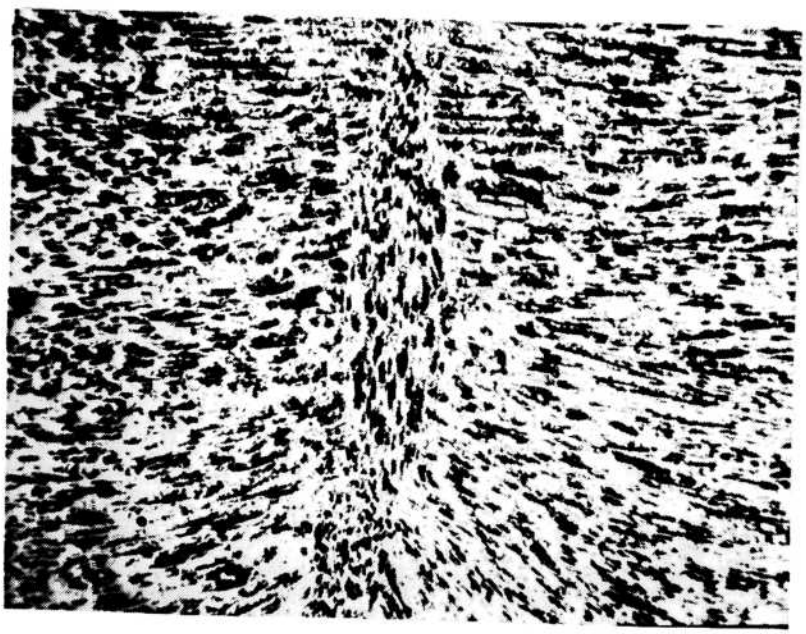

Fig. 7 b

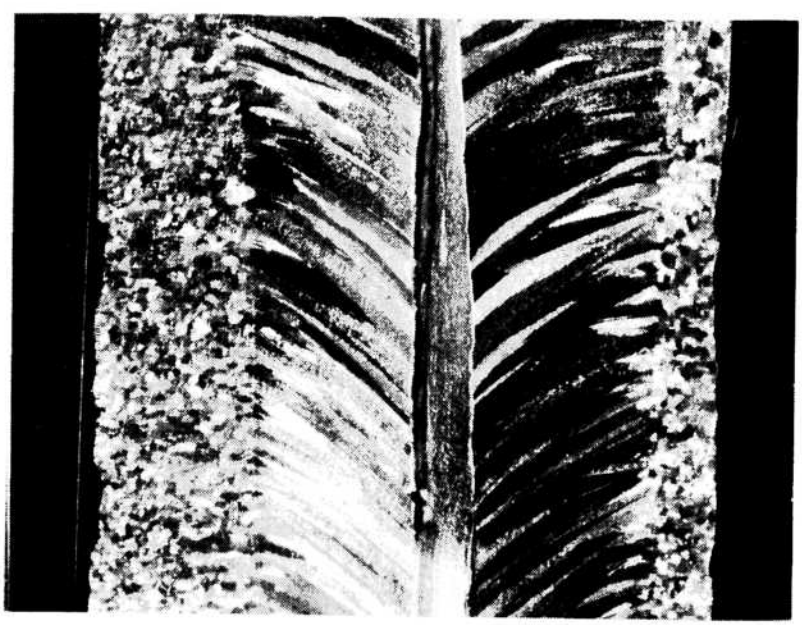

Fig. 8 a

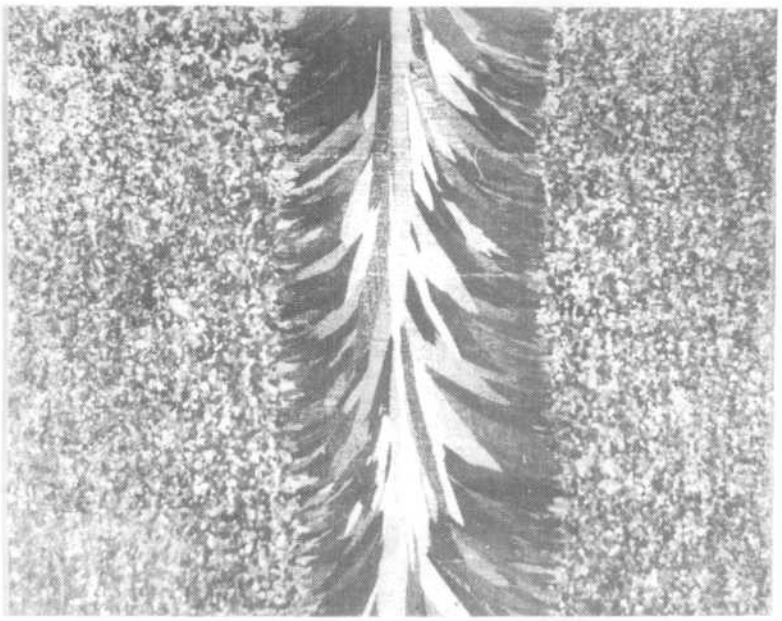

Fig. 8 b

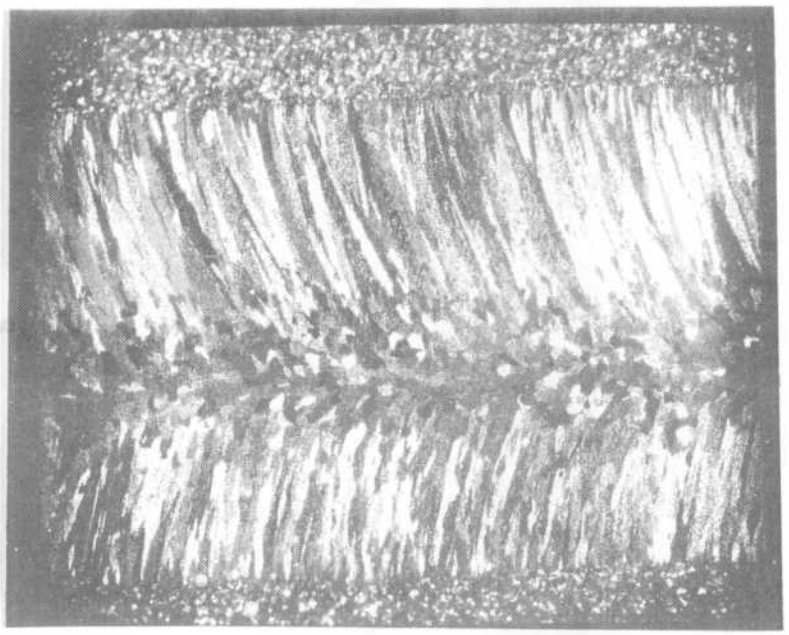

Fig. 9

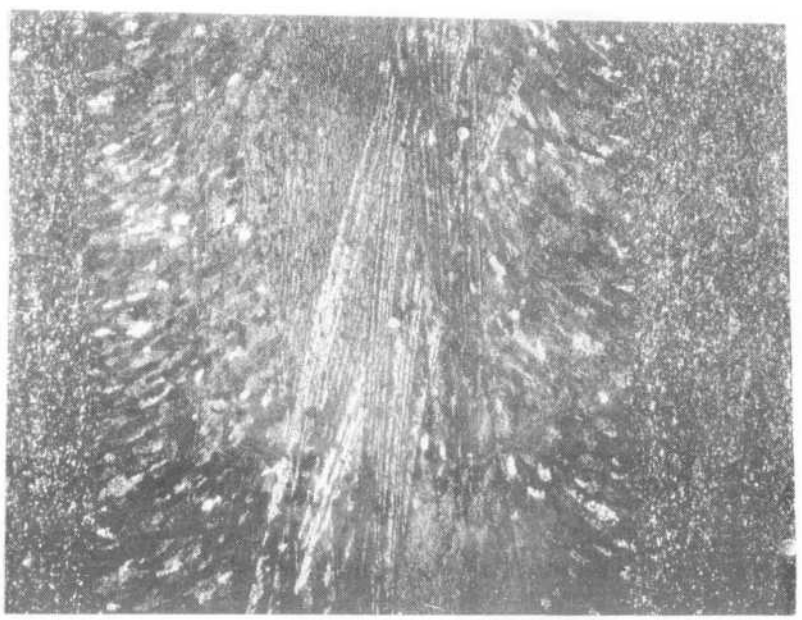

Fig. 10

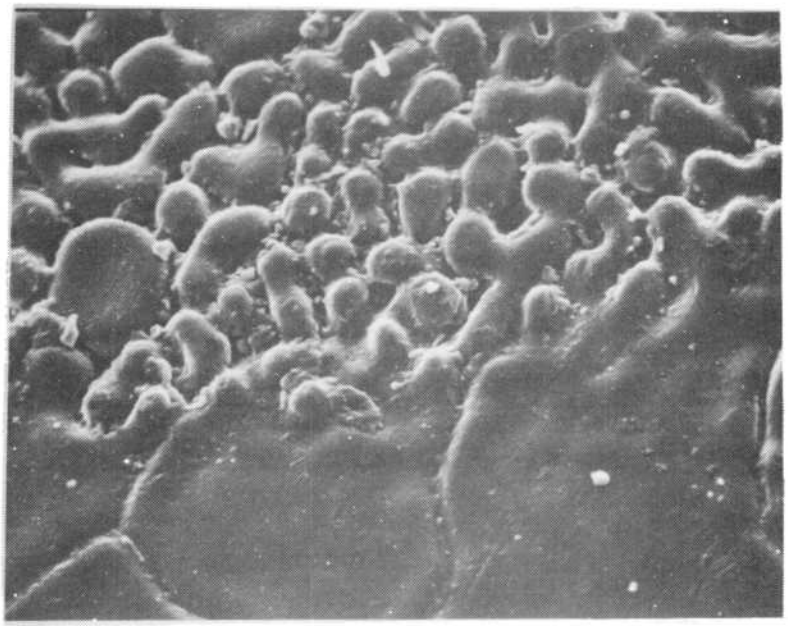

Fig. 11 a

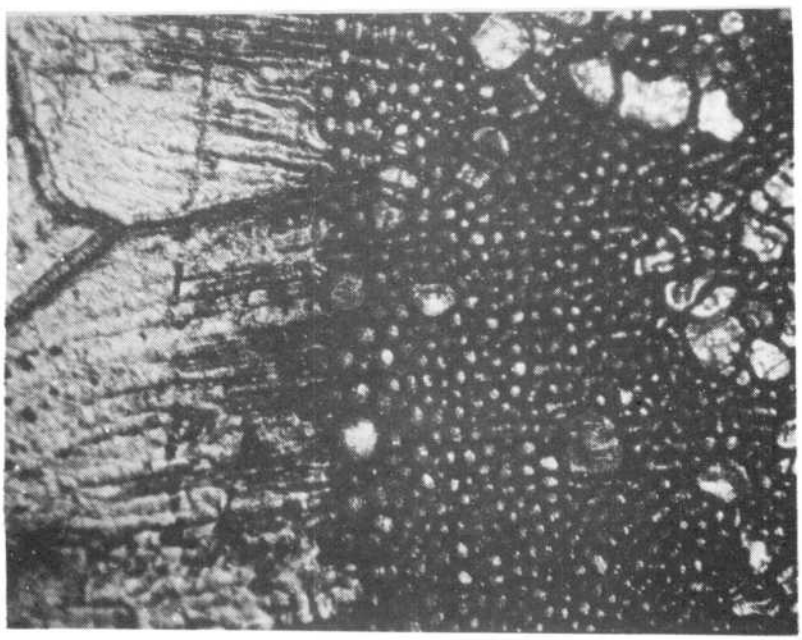

Fig. 11 b

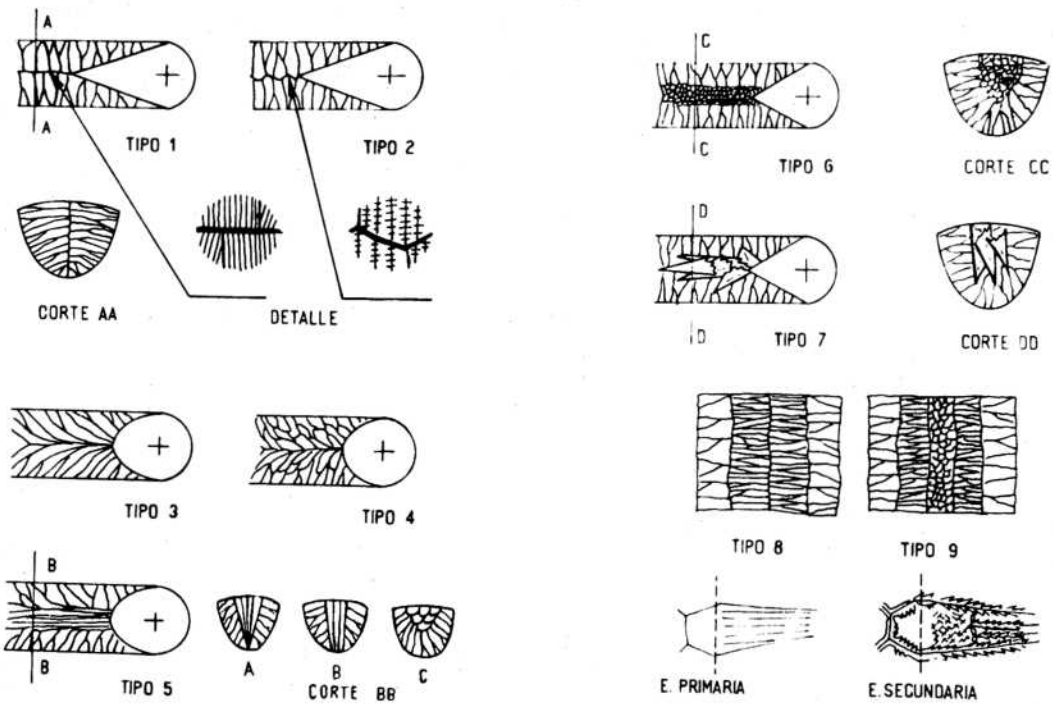
A
A
TIPO 1
TIPO 2
CORTE AA
DETALLE
TIPO 3
TIPO 4
B
B
TIPO 5
A
B
C
CORTE BB
C
C
TIPO 6
CORTE CC
D
D
TIPO 7
CORTE DD
TIPO 8
TIPO 9
E. PRIMARIA
E. SECUNDARIA

Fig. 12

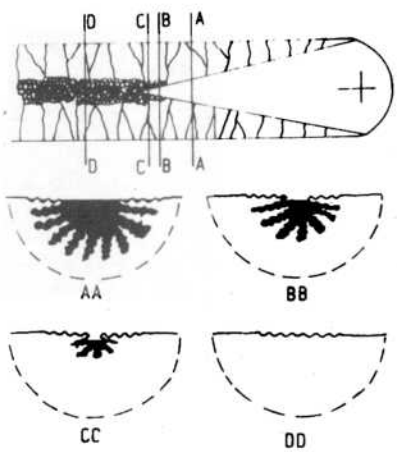
D
C
B
A
D
C
B
A
AA
BB
CC
DD

Fig. 13

-4-

"THE INFLUENCE OF THE WELDING MACROSTRUCTURE ON ALUMINIUM HOT - CRACKING"

by M.E. Saggese, M. Solari and H. Biloni

THE INFLUENCE OF THE WELDING MACROSTRUCTURE ON ALUMINUM HOT CRACKING

Ma. E. Saggese-Miraglia: INEND. Comisión Nacional de Energía Atómica (CNEA) Argentina.

M. Solari: Departamento de Materiales. CNEA.

H. Biloni: Director del Proyecto Especial Sobre Aluminio y Cobre. OAS--CNEA.

1 - INTRODUCTION

Hot cracking is a type of failure that can appear in al most all alloys when they are welded by any fusion process. It is generated by stresses arising both from the solidification contraction and the restraint provided by the joint. Additional restraint may be introduced by externa devices. Several works[1,8] correlate the structure developed during the solidification process, the composition of the weld, the geometry of the pool and the stresses developed during the process. They can by summarized as follows.

i) During the solidification process between liquidus and solidus temperatures of the alloy, the mushy zone of the weld is formed by a dendritic network with solute-enriched liquid around it. For $k_0 < 1$ this enriched liquid solidifies with a lower point of fusion and non-equilibrium phases or eutectics with a low melting point usually appear.

ii) Maximum segregation is achieved at the grain boundaries of the crystals having an interdendritic segregation as a result of the solidification process. In systems where the energy associated with the grain boundaries (σ_{SS}) is higher than twice the interfacial Solid-Liquid energy (σ_{SL}), the whole interfacial energy of the system is minimized through a mechanism consisting of penetration of the liquid through the grain boundaries.

iii) High velocity welds with a tear drop shape of the pool are more susceptible to hot cracking than others presenting elliptical pools resulting from low welding speed. The difference is attributed to the relationship existing between the columnar grains and the encounter angle

Under high speed conditions a very high encounter angle develops and the solute rejected at the solidification front, as well as the impurities present in the liquid, are trapped in the weld centerline As a consequence a high segregation arises. On the other hand elliptically shaped pools do not usually present a centerline segregation and as a consequence the danger of centerline hot cracking practically does not exist.

From the preceding items the cracking phenomena results in a combination of high segregated continous regions (namely at the centerline grain boundaries and interdendritic spaces), with solidification contraction during the completion of the mushy zone, contraction stresses developed in the cooling solid and an inadequate liquid feeding along the interdendritic spacings. The result is a concentration of stresses in a relatively small amount of solid regions triggering the conditions for the crack propagation.

The present paper is concerned with aluminum welds presenting an axial type of macrostructure, characterized by an elliptically shaped pool and grains that grow near the centerline, parallel to the welding direction and which, as a consequence , stop the columnar structure developed epitawially from the base metal[9]. The susceptibility to hot cracking of this structure will be established through a careful examination of the relationship existing between the macrostructure and the segregation substructure developed during the solidification process.

II - EXPERIMENTAL

a)Materials: TABLE I specifies the thickness and composition of the two sheets of commercially pure aluminum used in the experiments.

b)Equipment: A commercial power source able to operate in the DC or AC mode and with HF incorporated in order to start the arc, was used . With this equipment it was possible to select the current intensity as well as to control the upslope rate, upslope time, welding current, welding time, downslope rate, downslope time, final current (in order to control the cooling rate of the final part of the bead) and the final time. The welding torch travelled automatically in a range between 0 and 15 $\frac{cm}{min}$

c) Welding procedure: Beads on plates with continous HF and AC, where performed. The electrode used was tungsten thoriated and water refrigerated. Argon was used as the shielding gas. Previously to each operation the plates were cleaned with acetone and brushed. TABLE II sumarizes the welding procedure.

d) Metallographic techniques: Metallographic analysis was performed on the welding plane. The etchant used was: HCl:50cc; HNO_3:47cc; HF: 3cc. The etching time was used as a variable in order to regulate the proper detection of the segregation substructure and the macrostructure.

e) Special metallographic techniques:

e_1) Microanalysis: With a CAMECA MS46, X Ray images of Si and Fe were performed. In all the cases the samples were carefully polished until a diamond paste finish.

e_2) Surface observations: In order to obtain a proper view of the surface relief associated with the welding and the cracks a scanning microscope PESM 500 was used.

III - RESULTS

Through the experimental conditions reported in TABLE II the weld pools obtained had elliptical shapes. The shape of the solidification front can be inferred from the superficial ripples of the beads. Fig. 1 shows a SEAM micrograph of one of the cracked beads. This figure is considered representative of the experiments performed. For the heat inputs used (see TABLE II), the macrostructure was an axial type.

The hot cracks observed were located in two preferential places: the central line between two axial grains (Fig. 2a) and the encounter line of the columnar grains with the axial or central grains (Fig. 2b). A metallographic study of the segregation revealed that these places presented a higher and quasi-continous segregation when compared with the rest of the structure (Fig. 3)[9]. The X Ray images of cracked beads also confirmed a higher concentration of Fe and Si, in those regions. The observations of the crack surfaces with the SEM permits the following description:

i) A direct correspondence between tears on one face and adhered parts of the other part of the another face of the crack (Figs. 4a and b)

Fig. 5 shows with more detail the planar decohesion observed at different depths. The fracture surfaces show an axial celular dendritic structure decanted during the cracking process.

ii)Fig. 6 shows the distribution of the plastic deformation from the center to the tip of the crack. The same figure also shows the plastic deformation continuing in the non-cracked metal.

iii)Fig. 7 Shows the surface of a crack at a zone of minimum plastic deformation. The rounded off structure characteristic of decanted cellular dendritic morphologies, can be seen.On the other hand Fig. 8 corresponds to a place with a high amount of plastic deformation, near the tip of the crack.

IV - DISCUSSION

Upon review, as was pointed out in the Introduction the hot crack sensitivity is related to the shape of the weld pool[8] Elliptic pools obtained through a low welding speed would not be susceptible to crack initiation. The results of the present work seems to be in contradiction with that statement. However it is necessary to take into consideration that the structure obtained in the heat input range used was an axial macrostructure. This type of macrostructure develops an elliptical pool but presents at the center of the weld one or several grains growing axially parallel to the welding direction (see Fig. 2). Those grains present different characteristics from the segregation point of view, when they are compared with the columnar grains of the macrostructure. Metallographic analysis and microanalysis show that an almost continuous segregation exists associated with the grain boundaries of the central axial grains and at the limit between the columnar grains and the crystals. The origin of this segregation may be visualized as follows: the columnar grains from the base metal reject solute in front of them. Because they are growing with a low encounter angle, as a result of the elliptical pool, if the columnar growth is completed no centerline appear. However the existence of axial central grains growing in an enriched liquid change the situation in two ways: i) a terminal transient of solute distribution appears at the region where the columnar grains are

stopped by the axial crystals; ii) a high grain boundary segregation is favoured. The results in both cases is the quasi-continuos segregation arising from a tear drop shape of the weld metal pool. As a result, the conditions necessary for the development of hot cracking are quite similar; due to the low mechanical resistance of the liquid film the stresses concentrate in the few solid bridges. When they fail,a crack appears. In addition the contraction stresses have their maximum component in the direction perpendicular to the central grain boundaries, favouring the failure.

The present work suggests that in order to prevent hot cracking susceptibility, it is necessary to control the shape of the pool but also the segregation distribution that is determined by the weld macrostructure.

Concerning the plastic deformation associated with the cracks, it is necessary to consider:

i) At the central zone of a crack no deformation appears and soft rounded surfaces are observed. This suggests that dendrites growing from both crack faces in the liquid entrapped do not fill the space developed. As a consequence a decanted type of cellular dendrites appears.

ii) Towards the tip of the crack the surfaces show more and more tears and a larger amount of plastic deformation. This may be due to the appearance of the contraction stresses forcing the weld bead to deform plastically before cracking and the existence of a high number of solid bridges together with a less amount of liquid due to an inefficient local feeding.

The heterogeneous distribution of plastic deformation may then be a consequence of two mechanism operating during the propagation of the crack. At high temperature the cracks may grow partially by liquation of the grain boundaries, provided the relationship $\gamma_{SS} < 2\gamma_{SL}$ is accomplished. This is very difficult to evaluate taking into account the problems existing in order to measure the interfacial free energy as well as the rather unknown influence of minor amounts of impurities on their values ( ). At lower temperatures this mechanism would stop

and then the solid bridges would have to stand the stresses imposed by the cooling of the bead.

V - CONCLUSIONS

1) Elliptical pools associated with an axial type of macrostructure are susceptible to hot cracking.

2) The cracks develop at the axial grain boundaries and at the limit between the columnar structure and the axial grains.

3) The metallographic and microanalysis studies show an almost continuos segregation in those regions.

4) The origin of the hot cracking is similar to the center line hot cracking appearing in columnar structures, associated with a tear drop shape of the weld pool. This indicates that not only the geometry of the weld pool must be taken in consideration, but also the relationship existing between the macrostructures and the solute segregation.

5) The analysis of the cracks shows the presence of an heterogeneous plastic deformation.

REFERENCES

1.- "Solidification Structures and Properties of Fusion Welds" G. DAVIES, T. GARLAND. Int. Met. Rev. 1975, V. 20. Review 190,83.

2.- "Welding Metallurgy" GEORGE LINNERT. Third Edition, Volume 2. A.W.S. 1967

3.- "Manual de la Tecnología de la Soldadura por Arco". H. KOCH Ed. Reverté S. A. 1965

4.- "Generalized Theory of Super Solidus Cracking in Welds (and Castings)" J. C. BORLAND British Welding Journal, August 1960 508.

5.- "Fundamentals of Solidification Cracking in Welds" Part 1 J. C. BORLAND Welding and Metal Fabrication. January/ February 1979, 19.

6.- "Fundamentals of Solidification Cracking in Welds" Part 2 J. C. BORLAND. Welding and Metal Fabrication. March 1979, 99.

7.- "Control of the Solidification Process During Submerged Arc Welding" T. EDVARSON. Presented at the Sheffield Int. Conf. on Solidification and Casting. 1977.

8.- "Segregation Hot Cracking in Low Alloy Quench and Tempered Steels". W. SAVAGE C. LUNDIN R. HRUBEC. Welding Journal September 1968, 420-S.

9.- "Macrostructures of Fusion Welds" T.E.PEREZ M.SOLARI and H. BILONI. Work to be published.

MATERIAL	THICKNESS	Fe	Si	Ga	Pb	IMPURITIES
	cm	wt%	wt%	wt%	wt%	wt%
A	0.25	0.27	0.12	0.03	0.05	0.005
B	0.30	0.13	0.13	0.03	0.05	0.005

TABLE I

Base Metal	Materials A and B
Electrode (W-10%)	0.235 cm Ø
Nozzle (Alumina)	0.787 cm int. Ø
Current intensity	87 /to 155 Amp. (A.C.)
Voltage	16 to 18 V
Welding speed	20 to 60 cm/min.
Heat imput (H.I.=IV/v)	2.50 to 4.20 KJ/cm

TABLE II

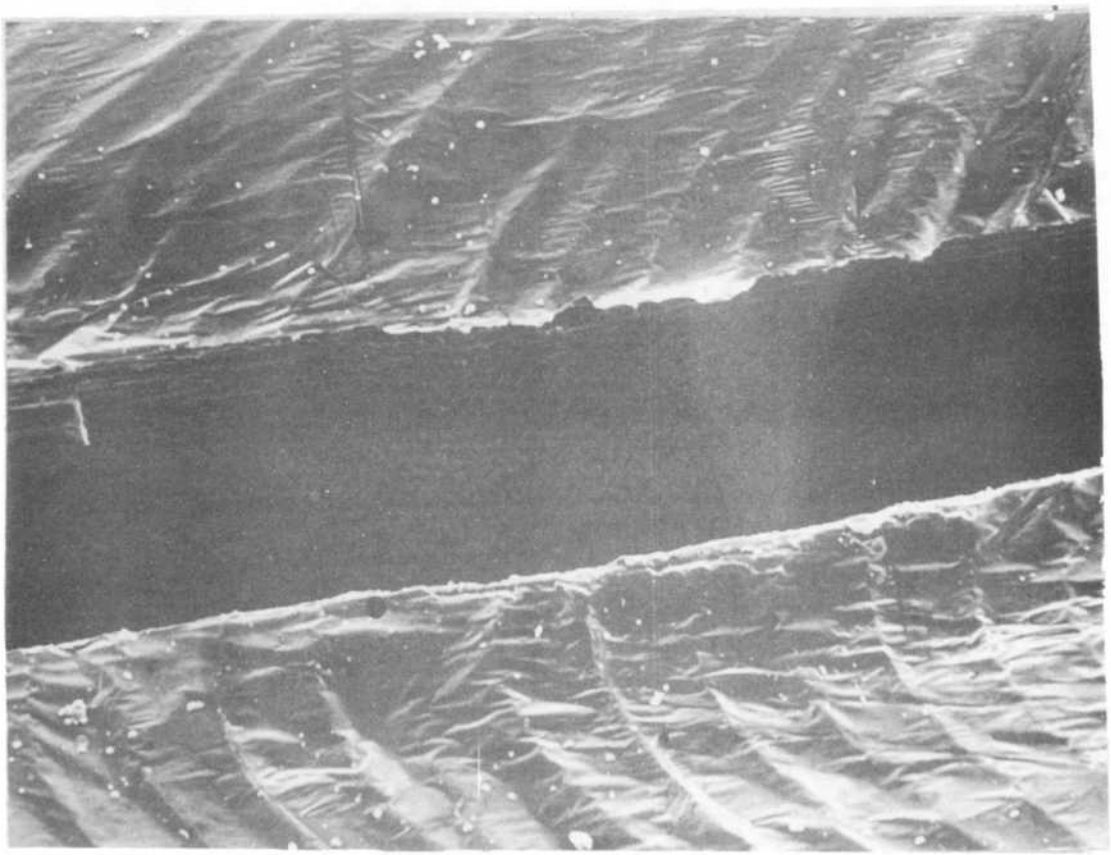

Fig. 1 Hot crack in as welded metal surface. Notice the elliptical type of the pool revealed by the surface ripple

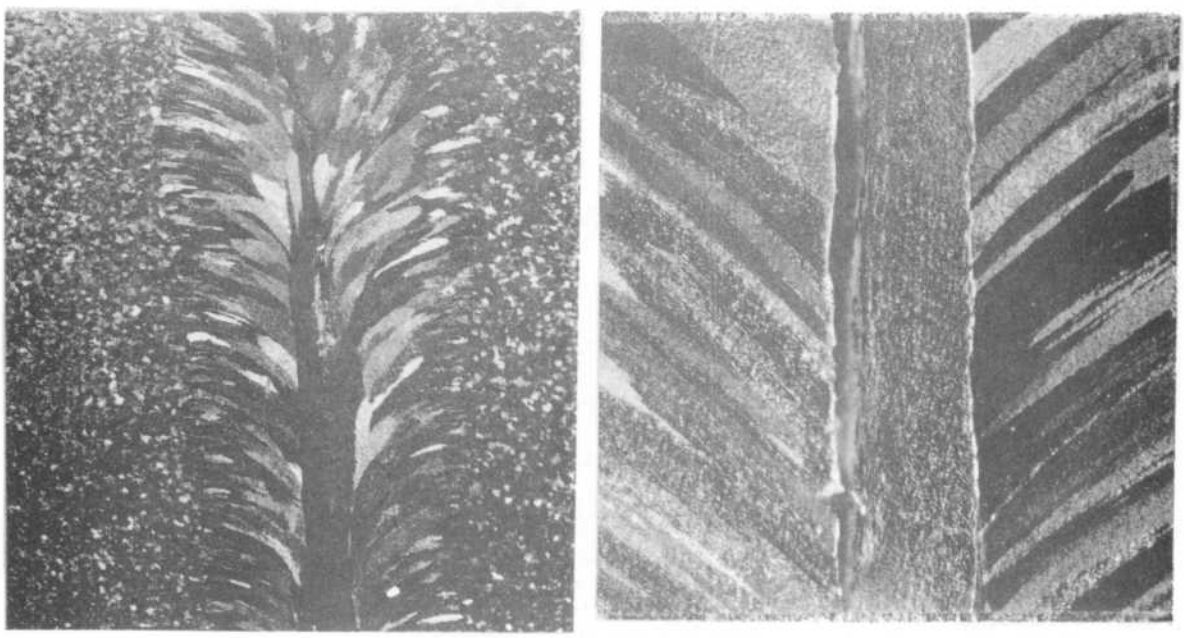

a b

Fig. 2 Axial macrostructures presenting hot cracks. a)Between two central grains, X4,5. b)At the limit between a central grain and the columnar front, X14.

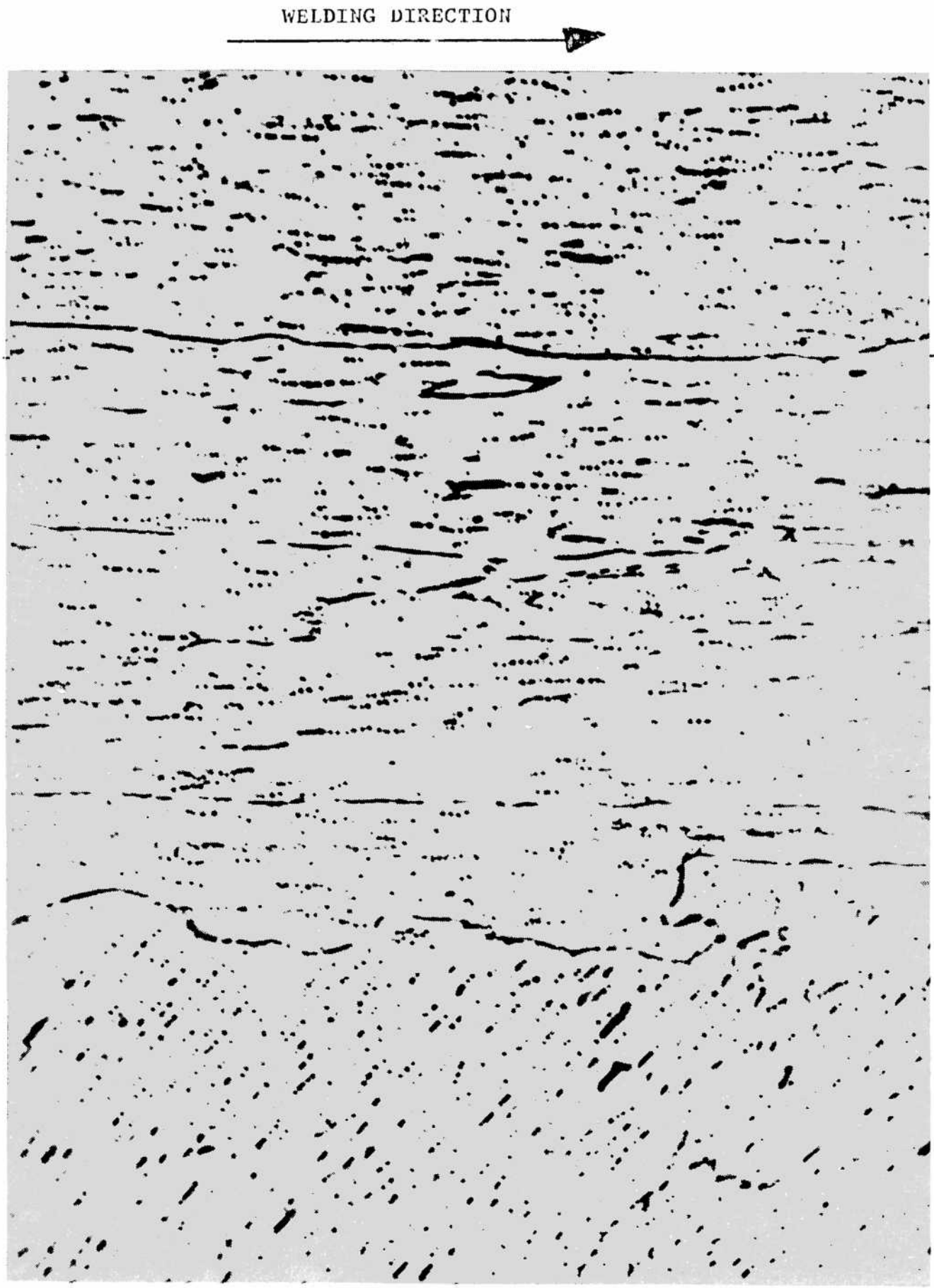

Fig. 3 Microsegregation in an axial structure. Notice the continuos segregation at the grain boundaries and at the limit between the columnar region and the axial grains. X400.

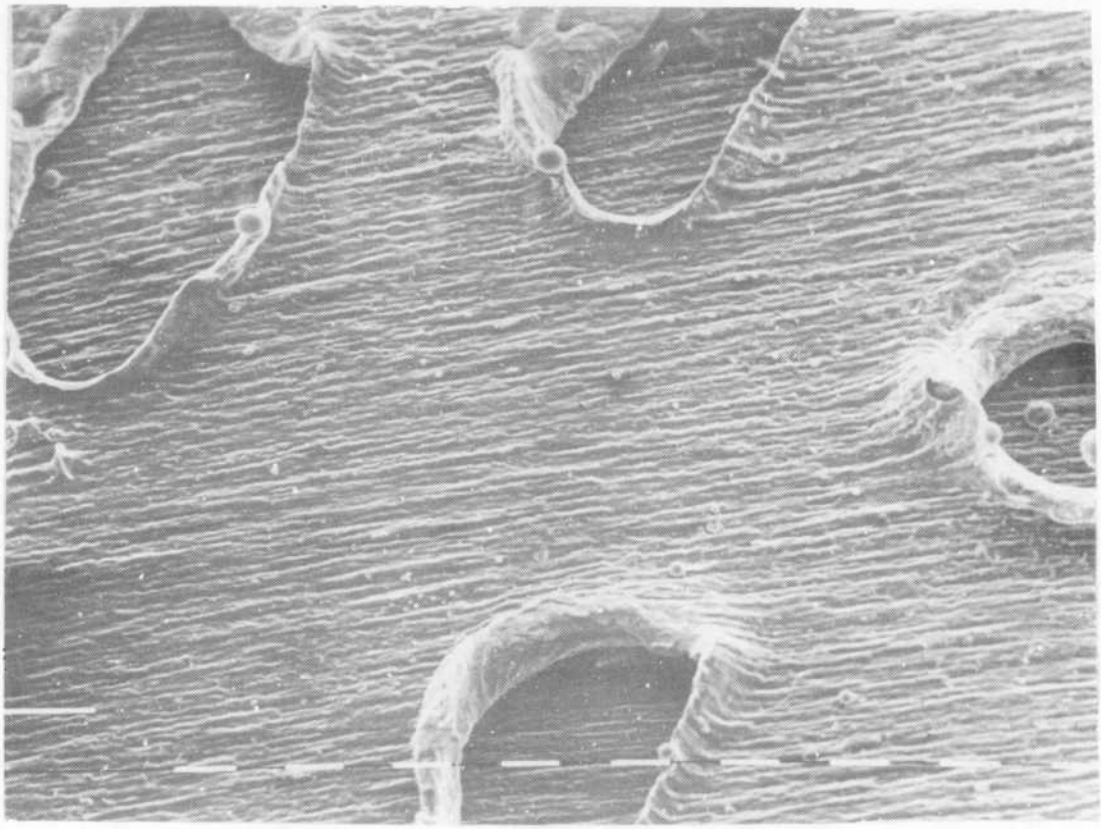

a

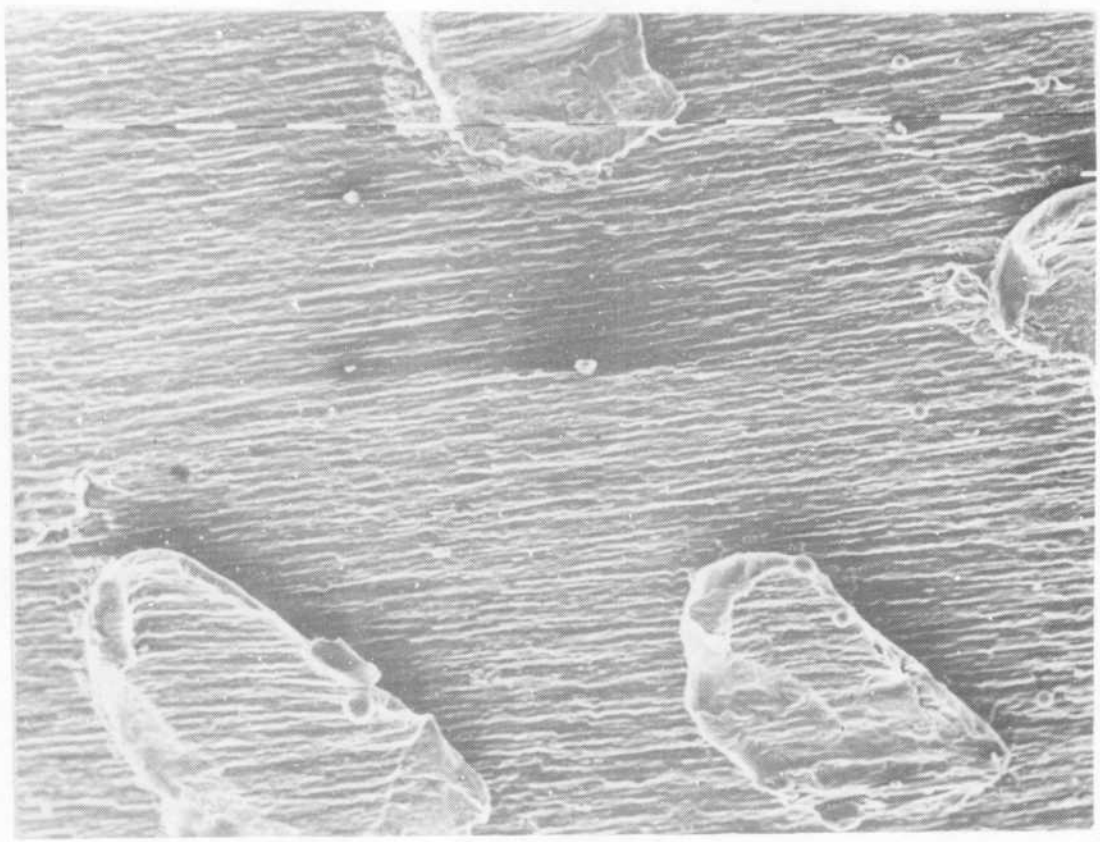

b

Fig. 4 Corresponding fracture surfaces of a hot crack located at the boundary of a central grain. As welded X 100, SEM micrograph.

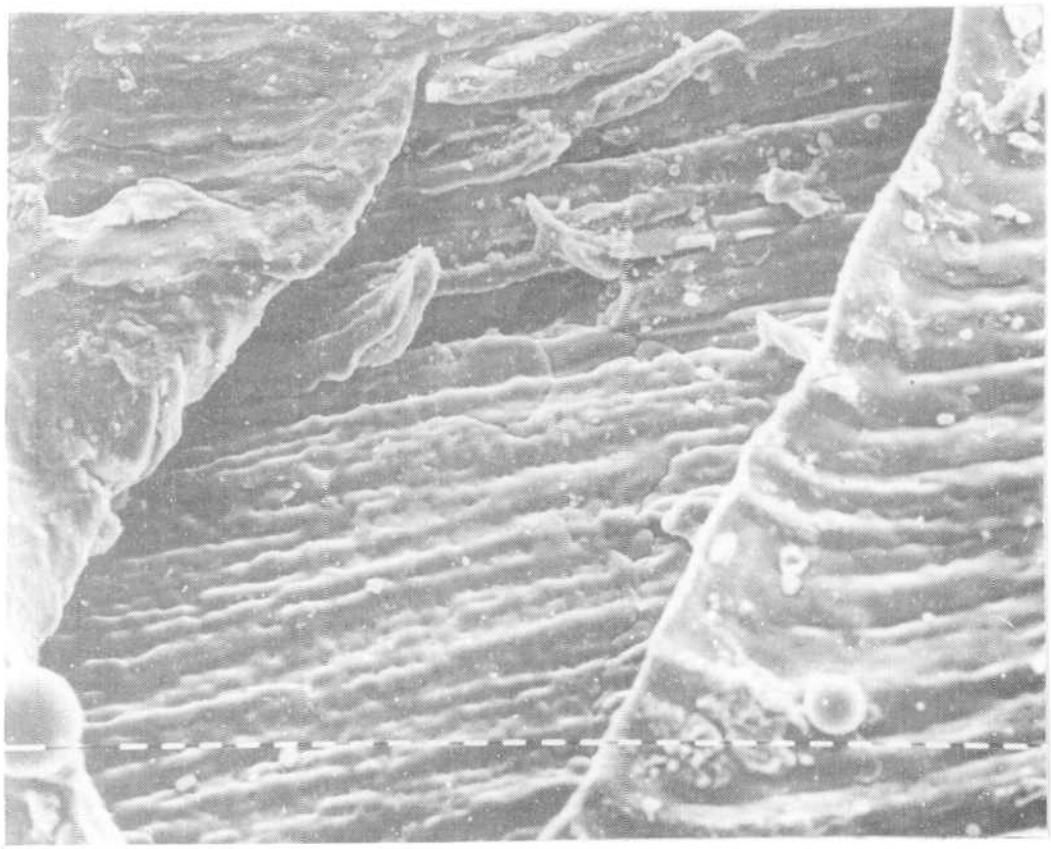

Fig. 5 Detail of Fig. 4 X400.

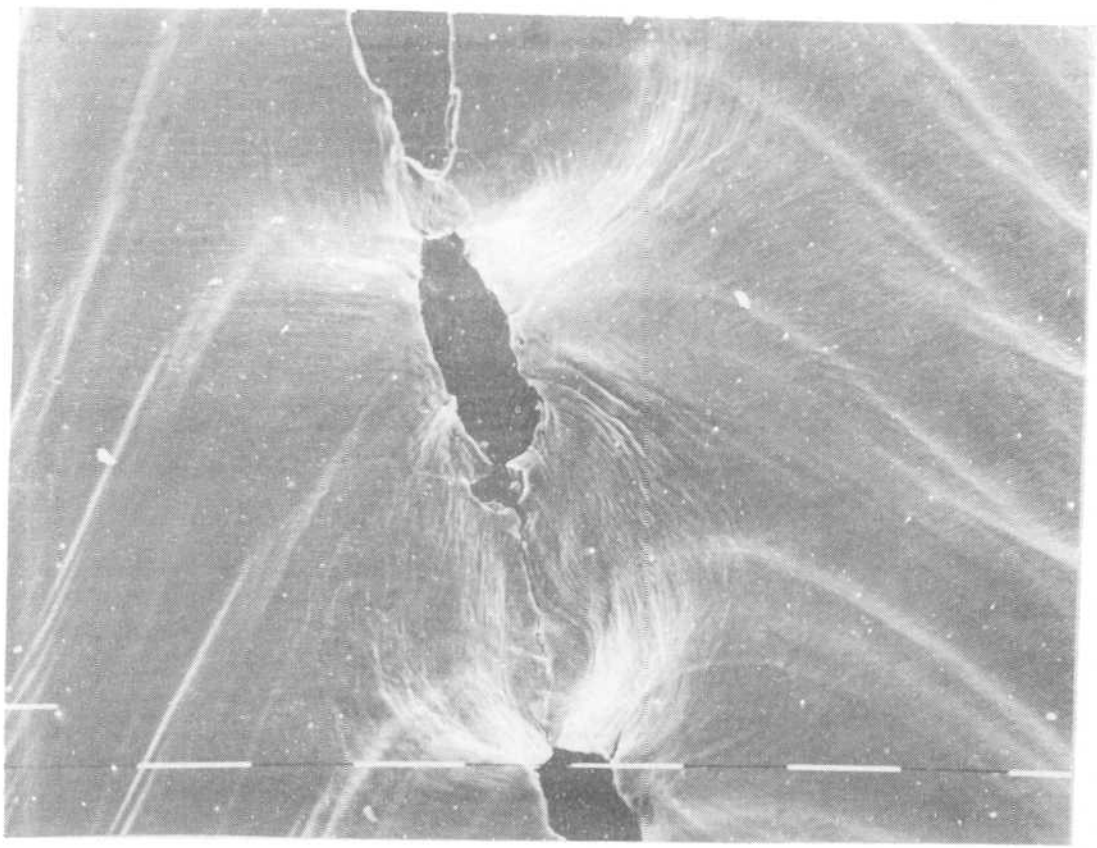

Fig. 6 Plastic deformation associated to an axial structure hot cracked at the centerline. As welded. X160 SEM micrograph.

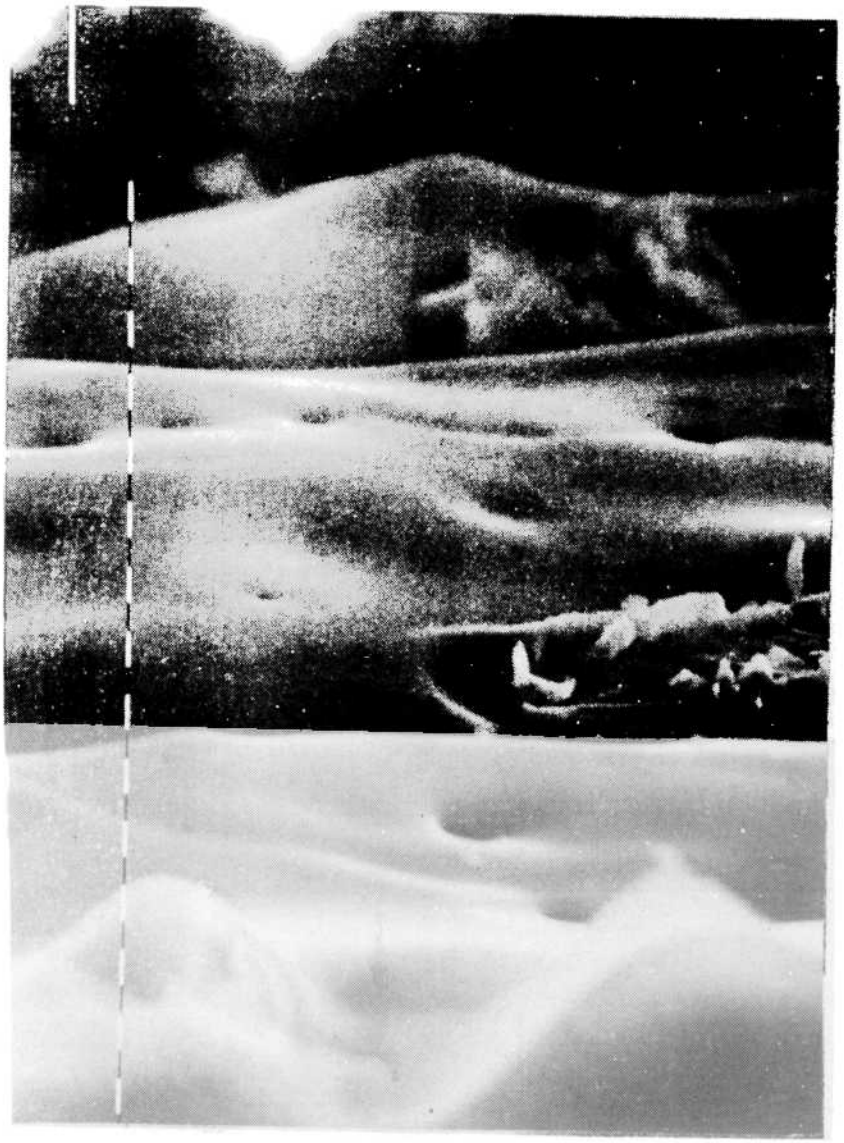

Fig. 7 Surface of a crack far from the tip As welded X4000SEM micrograph.

"METALLOGRAPHIC SULPHUR DETERMINATION BY SEM IN AUSTENITIC STAINLESS STEEL WELD METAL"

by J. I.Morgenfeld, M. Solari and Ovejero Garcia

Technical Note:

METALLOGRAPHIC SULPHUR DETERMINATION BY SEM IN AUSTENITIC STAINLESS STEEL WELD METAL

By J.I.Morgenfeld, M.Solari and J.Ovejero-García

J.I.Morgenfeld is with the Comisión de Investigaciones Científicas de la Provincia de Buenos Aires, and M.Solari and J.Ovejero-García are with the Departamento de Materiales de la Comisión Nacional de Energía Atómica, Buenos Aires, Argentina.

Technical Note: METALLOGRAPHIC SULPHUR DETERMINATION BY SEM IN AUSTENITIC STAINLESS STEEL WELD METAL

Julio Morgenfeld, Mario Solari, José Ovejero-García

INTRODUCTION:

Sulphur distribution in weldments is of great interest because it is associated with several phenomena : corrosion, mechanical resistance, intergranular brittleness, hot cracking, etc.(1)

Probably the most common method to reveal segregated sulphur widely used in industry is the one developed by Baumann in 1906 (2). This technique permits the detection of sulphur in a direct way. However, the silver bromide crystals of photographic paper are several microns in size, so the resolution achieved by this method is restricted.

Recently, a new metallographic technique was developed - called microprint Baumann or sulphur microprint - which reveals sulphur in a direct way even at the electron microscopic scale (3).

In the CNEA's Materials Laboratory, the hot cracking of austenitic stainless steel is investigated using the solidification theory background and the Varestraint test. The aim of this work is to analize the relationship between operative variables and the mechanism responsible for hot cracking, taking into account microstructural features. In this framework, the results of the present investigation indicate that a sulphur microprint is useful to reveal sulphur segregation in austenitic stainless steel weld metal. As a consequence it appears to be an excellent tool in the hot cracking research field.

BACKGROUND:

During welding the molten weld pool does not freeze according to equilibrium conditions and thus, during metal alloy cooling from the liquid state, a solute pile-up in front of the solid-liquid interface may appear. So, an instability is originated, which produces morphological changes. The Constitutional Supercooling criteria developed by Chalmers (4), permits the determination of interface instability conditions, besides justifying the fact that the dendritic growth can develop towards the liquid pool center in a temperature gradient direction.

The first visible instability signals connected to the interface are depressions, called nodes (5), allowing its metallographic detection by special techniques.

In a typical fusion weld the solid surface in contact with liquid metal grows adopting a cellular or dendritic shape, with the object of eliminating the constitutional supercooling by redistributing the solute in front of the interface. The result is a short range segregation - microsegregation - located in the interdendritic spacing.

Microsegregation can appear in correlation with nonmetallic inclusions, microporosities and microshrinkage.

On the other hand, the relationship between solidification structure and hot cracking is well known. In general, hot cracking is caused by the combination of two factors : i) mechanically and/or thermally induced strain, and ii) crack susceptible microstructure. Welding parameter, rate of solidification, alloy composition and microsegregation are all factors which play an important role in the control of hot cracking associated with welding.

Sulphur can appear in the solidified weld metal as a solid solution as well as non-metallic inclusions. The strong sulphur segregation in the interdendritic spacing is due to its too low partition coeficient. Several authors showed that steels with the same chemical composition but with diferent sulphur content could have different behaviours in reference to its weldability.

The Fe-Cr-Ni stainless steels can solidify as austenitic dendrites as well as delta ferrite dendrites. Austenitic stainless steel weld metal normally has a duplex structure that contains varying amounts of ferrite. The delta ferrite can be associated with the interdendritic spacing as well as the cores of dendrites according to the cooling rate and composition. Extensive discussions have been published on the solidification behaviour and origin of ferrite in austenitic stainless steel weld metal. However, no one has been able to clearly establish the solidification sequences leading to the observed final microstructure of the weld metal (6),(13).

It is recognized that if sufficient ferrite is in the weld, the ferrite will effectively prevent hot cracking (7). The ferrite level that prevents cracking is found to be dependent on the impurity level, whereas for low P+S, little or no ferrite is required to prevent cracking. With ferrite contents greater than ferrite numbers 13 or 14 large amounts of P and S can be accomodated without cracking (8). Compared to phosphorous, sulphur has a much greater effect on high temperature cracking(9).

The importance of sulphur in hot cracking corresponds to its association with low melting point films as well as a ductility diminishment near solidus.

Taking into account the complex distribution of austenite

and delta ferrite (approx. 1 μm wide) as well as the micro-segregation associated with a fine dendrite arm spacing (approx. 5 μm) typical in weldments, it results that the electronic microprobe technique (limited by the probe size to 1 μm^3, and sensibility, doses higher than .3% in weight) is not capable of determining sulphur distribution in this fine scale. On the other hand, the epitaxial layers technique enables one to reveal segregation very accurately, but it is not possible to determine sulphur in a selective way.

Techniques for analysis of fracture surfaces with good depth resolution, such as Auger electron spectroscopy, are difficult to apply to austenitic stainless steels which resist intergranular fracture. On the other hand, X-ray mycroanalysis of thin foil specimens appears to be the best technique currently available for high spatial resolution analysis of the heavy elements in austenitic steels (10) (resolution of 30 nm). However, the applicability of this technique is limited by the method's complexity.

An alternative technique is high resolution autoradiography with radioactive sulphur S^{35}, which is also limited to laboratory studies.

The originality of the sulphur microprint is based on the association of the classic Baumann test with high resolution autoradiography, in which a silver bromide monogranular emulsion is deposited on the surface specimen.

The technique used in this work can be applied not only to massive pieces, with a conventional metallographic specimen observable by SEM, but to thin foils observable by scanning electronic transmition microscopy with a 150 nm resolution. It is possible to reveal the sulphur distribution with a very high

sensitivity; for example it has been reported that sulphur monoatomic layers were revealed.(12).

This technique can be useful in the study and solution of many problems in basic as well as applied investigations, such as stainless steel hot cracking.

MATERIALS AND PROCEDURES:

The stainless steel AISI 304L studied was used in the form of a 3 mm sheet. The experimental fusion welds used were performed with semi-automatic GTA with 11 volts and 90 amperes, in an argon atmosphere with 30 cfh flow and a travel speed of 30 cm/min.

The metallographic specimens were prepared according to conventional prectice. The upper surface of the welds were polished to the diamond stage. Then, two touches with automatic electrolitic polishing were performed using 20 volts during 10 sec; the reagent used was A2: 78ml percloric; 100ml Butilcellosolve, 700ml etanol and 120ml H_2O. Finally, an electrolitic attack with 10 % oxalic acid and 8 volts was performed.

SULPHUR MICROPRINT EXPERIMENTAL METHOD:

The sulphur microprint principles were detailed in a previous paper (3), so the following description will be brief.

The metallographic prepared specimen is covered with a nuclear emulsion thin film Ilford L4. Then a 10 % diluted sulphuric acid drop is deposited during 10 sec with the aim of producing SH_2 detachment and SAg_2 formation. After the operation of fixing and washing with distilled water, the specimen-emulsion

as a whole is observed by SEM. The SAg_2 appears superimposed on the microstructure as brilliant white grains. Thus it is possible to correlate the sulphur segregation with microstructural details.

RESULTS AND DISCUSSION:

As an initial step in the investigation of sulphur heterogeneity in weld metal, a study was carried out on austenitic stainless steel AISI 304L in order to observe sulphur microprint suitability.

Figure 1 is a photomicrograph of a transverse cross section of a weld bead showing a periodic sulphur segregation within columnar grains. This chemical heterogeneity corresponds to an interdendritic segregation resulting from a cellular dendritic growth. The SEM photomicrograph shows the SAg_2 brilliant white particles with a resolution of up to 300nm. The presence of this type of particle is associated with sulphur microinclusions or sulphur in solution. The dendritic arm spacing (das) is in the range of 5 µm. Flemings (11) has pointed out that the mechanical properties of cast metals are strongly dependant on this parameter. The das is a function of cooling rate and composition. It should be noted that das diminishes as the cooling rate increases. This parameter is a mesure of the size and distribution of the structural elements.

Figure 2 shows an area close to the fusion line of the above mentioned weldments at higher magnification. This photomicrograph shows sulfur inclusions in the segregated regions.

Preferential segregation at the structure nodes is shown in figure 3. The nodes correspond to real solute enriched liquid channels. When th interface instability condition is present, a tendency to balar e the solute rejection with a curvature change

occurs. Note that the solute and temperature difussion coefficients are very different, so the heat and mass transfer are balanced for a curved interface due to the different flow directions. The degree of segregation depends upon solute pile-up and interface curvature effects, solid state difussion and dendritic arms coarsening.

Figure 4 shows a high magnification detail of sulphur inclusions. A previous work (3) reported the possibility of revealing sulphur microprecipitation in the delta ferrite - austenite interface. Now, a part of the present work in austenitic stainless steel weld metal is the study of sulphur segregation in a delta ferrite - austenite interface using thin foil sulphur microprint specimens, observed by TEM.

CONCLUSIONS:

The experimental work performed reveals that the application of the sulphur microprint technique to the investigation of austenitic stainless steel weld metal allows the successful selective detection of sulphur segregation from the solidification process. This new technique becomes an important tool in the study of weld metal solidification and hot cracking. Aditionaly, the thin foil sulphur microprint observed by TEM will offer higher accuracy in the detection of sulphur segregation.

REFERENCES:

1.- R.Stout and W.Doty, "Weldability of Steels", WRC, N.Y.1971.

2.- R.Baumann, Métallurgie, 416, 1906.

3.- G.Moulin, J.Ovejero-García, C.Haut, M.Dadian et M.Acouturier, "La micro-empreinte Baumann a haute résolution pour la mise en

évidence de microsegregations de soufre à l'echelle de la microscopie électronique", Rev.Met. 11:627-632, Nov.1978.

4.- B.Chalmers, "Principles of Solidification", J.Wiley & Sons, N.Y. 1962.

5.- H.Biloni, G.F.Bolling and G.S.Cole, Trans.TMS-AIME 236, 1966

6.- H.Fredriksson, "The Solidification Sequence in an 18-8 Stainless Steel, Investigated by Directional Solidification",Metal. Trans. 3(11):2989-2997, Nov.1972.

7.- W.T.Delong, "Ferrite in Austenitic Stainless Steel Weld Metal", Weld.J.53(7):273s-286s, july 1974.

8.- J.A.Brooks and F.J.Lambert, "The effects of Phosphorus, Sulfur and Ferrite Content on Weld Cracking of type 309 Stainless Steel", Weld.J.57(5):139s-144s, may 1978.

9.- H.Homma, N.Mori and K.Shinmyo, "A Mechanism of High Temperature Cracking in Steel Weld Metals", Weld.J.58(9):277s-282s, sept. 1979.

10.- C.E.Lyman, P.E.Manning, D.J.Duquette and E.Hall, "STEM Microanalysis of Duplex Stainless Steel Weld Metal", Scanning Electron Microscopy 1:213-220, 1978.

11.- M.C.Flemings, "Solidification Processing", Mc Graw-Hill, N.Y. 1974.

12.- A.Larere, G.Moulin, J.Ovejero-García, C.Haut and C.Roques-Carmes, "Detection of Intergranular Sulphur Segragation in Commercial Nickel by High-Resolution Sulphur Microprint", to be published.

13.- J.C.Lippold and W.F.Savage,"An Investigation of Duplex Weld Solidification in Austenitic Stainless Steels", Weld.J.58(12): 362s-374s, Dec 1979.

LEYENDS TO FIGURES

1.- Cross section of a weld bead showing a periodic sulphur segregation within columnar grains.(800 X).

2.- Sulphur inclusions in the segregated regions of an area close to the fusion line. (1200 X).

3.- Preferential segregation at the structure nodes (3200 X).

4.- High magnification detail of sulphur inclusions (3200 X).

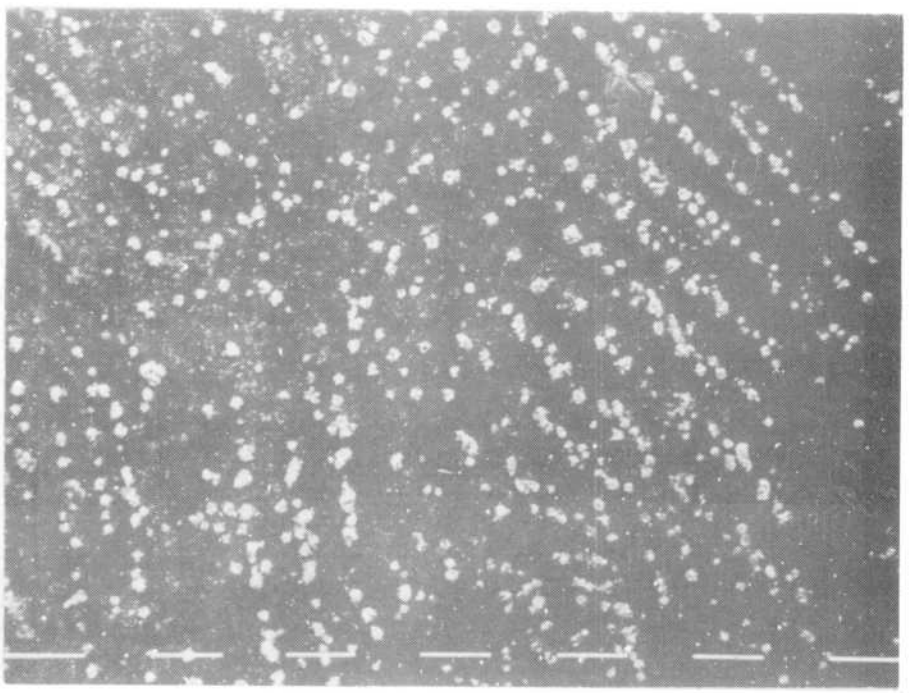

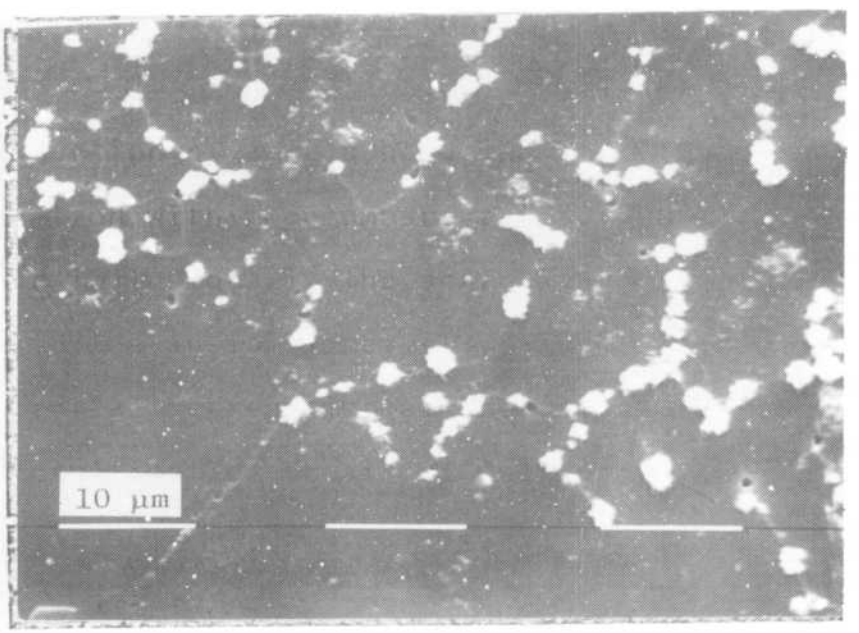

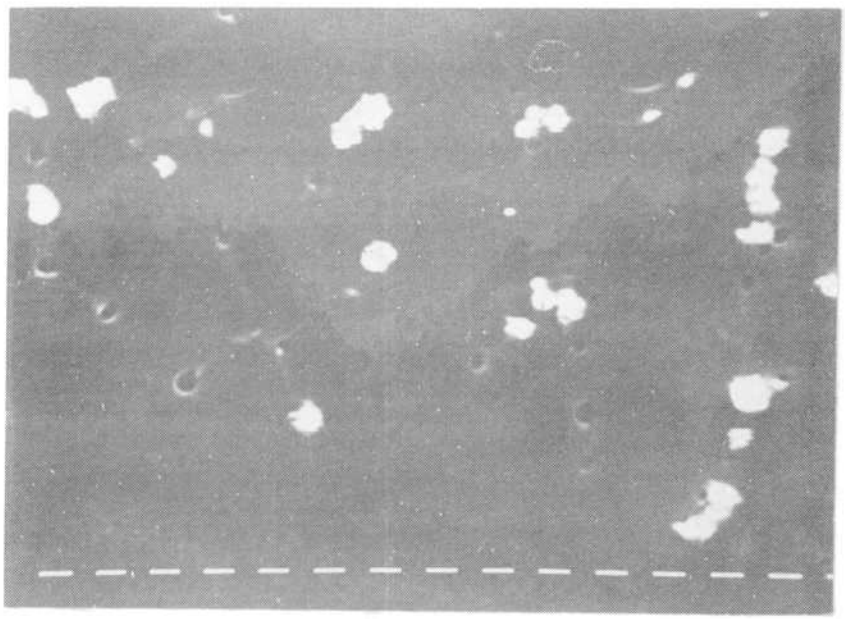

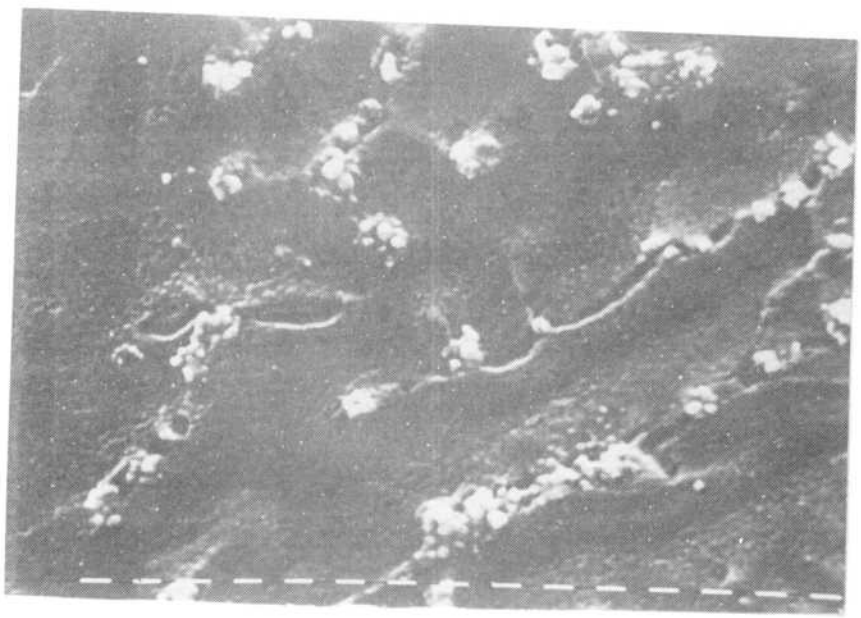

-6-

"MICROSEGRATION IN CELLULAR AND
CELLULAR DENDRITIC GROWTH"

by M. Solari and H. Biloni

Journal of Crystal Growth 49 (1980) 000–000

MICROSEGREGATION IN CELLULAR AND CELLULAR DENDRITIC GROWTH

Mario SOLARI
Departamento de Materiales, Comisión Nacional de Energía Atómica, Buenos Aires, Argentina

and

Heraldo BILONI
Director Programa Multinacional de Metalurgia OEA–CNEA, Buenos Aires, Argentina

Received 1 October 1979

On the basis of Flemings' microsegregation model and the work done by Burden and Hunt describing cell tip composition and undercooling as a function of the growth variables, a general microsegregation equation is proposed. The particular cases consider diffferent conditions: (i) cellular solidification; (ii) columnar growth; (iii) solidification at high speed and (iv) processes where the solidification rate changes during the process, as in welding.

1. Introduction

Extensive work has been done to develop a theory able to predict microsegregation in cellular and cellular dendritic growth. As Flemings pointed out [1], two different approaches were used in the literature. Meanwhile, several authors [2–5] developed analysis for dendritic growth considering only the dendrite tip and its growth into an isothermal or isoconcentrated liquid. Flemings and coworkers [6] neglected dendrite tip-related phenomena and concentration processes occuring behind the tip during solidification of alloys melts. This led to quantitative understanding of a variety of solidification phenomena, including microsegregation.

On the other hand, Burden and Hunt [7–9] proposed a model in order to explain the variation in cellular or dendritic tip temperatures with velocity and temperature gradient. The model predicts that undercooling can be considered to occur as a result of the build up of average solute concentration ahead of the growth front, depending mainly on the imposed temperature gradient, together with an additional term necessary to satisfy mass balance at the interface. Flemings pointed out [1] that the basic ideas coming from the two different approaches can be unified and that the result would be a base on which to study the dendrite growth process. In that frame the present paper is an attempt to propose a general equation able to consider the different solidification conditions arising in different technological processes.

2. Proposed model

Fig. 1 corresponds to the model for dendritic growth, proposed by Flemings and coauthors [10]. In the present work an extra assumption related to the cell of dendritic cell tip is made.

The extra assumption is that there exists an undercooling in front of the interface not only as a consequence of a build up of solute but also as a curvature effect of the solid–liquid (S–L) interface. Kinetic undercooling is not considered.

From Burden and Hunt's model the composition of the dendrite tip (C_t) can be calculated:

$$C_t = C_\infty(1-a) + bC_\infty , \tag{1}$$

where

$$a = G_L D_L / m_L R C_\infty , \tag{2}$$

$$b = [-2KR(1-k_0)/m_L D_L C_\infty]^{1/2} \tag{3}$$

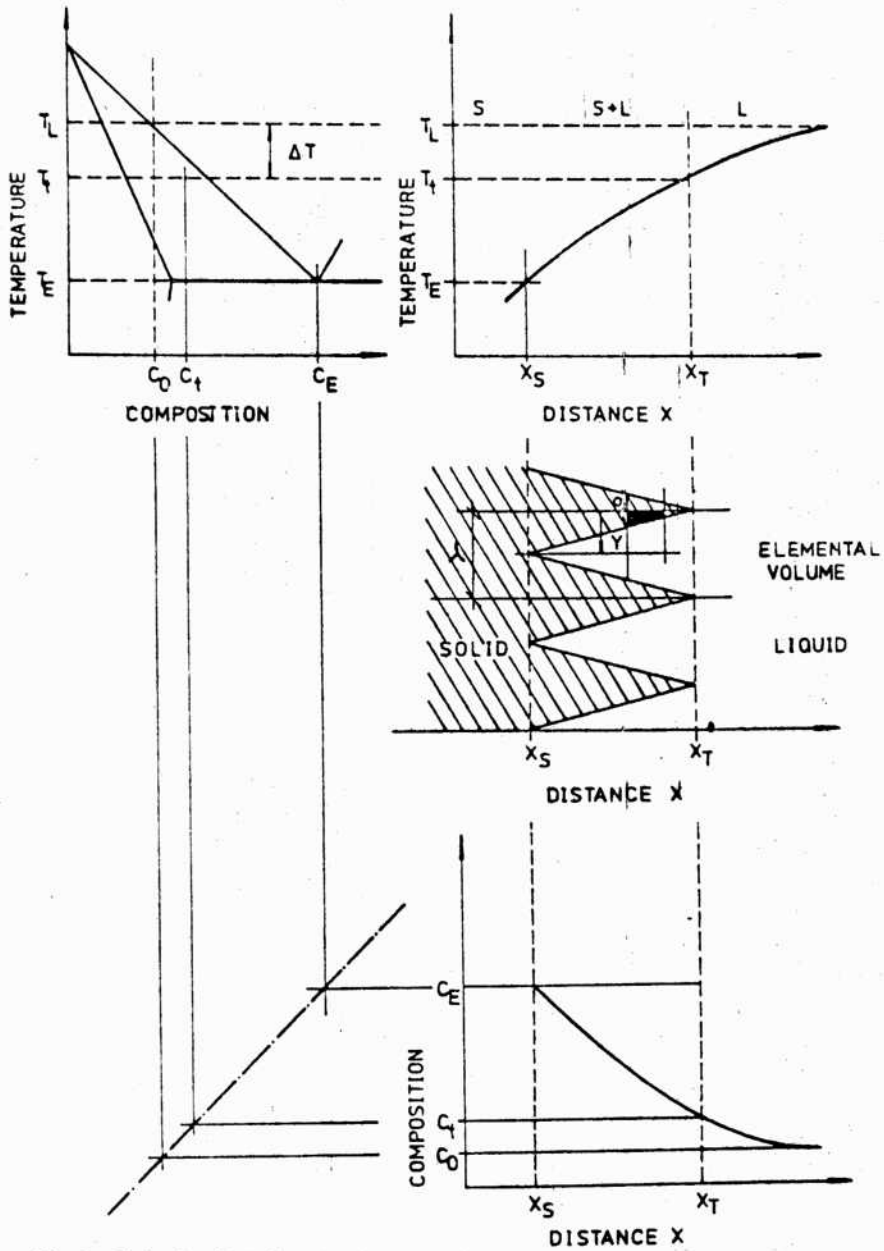

Fig. 1. Conceptual model of cellular dendritic freezing showing: (a) portion of the phase diagram; (b) schematic temperature distribution in the melt; (c) distribution of solute within the liquid of the mushy zone; (d) representation of platelike, unbranched dendrites showing the position of a characteristic volume element. From ref. [10].

The undercooling in front of the interface as a function of the freezing conditions and alloy properties is [8]

$$\Delta T = \frac{G_L D_L}{R} + 2^{3/2}\left[-\frac{m_L(1-k_0)\,C_\infty K}{D_L}\right]^{1/2} R^{1/2} \quad (4)$$

In expressions (1)–(4): C_∞ = liquid composition far from the S–L interface; G_L = liquid gradient; K = curvature constant = $\sigma/\Delta S$, where σ = S–L interface free energy and ΔS = fusion entropy of the pure metal; k_0 = partition coefficient; and m_L = liquidus slope.

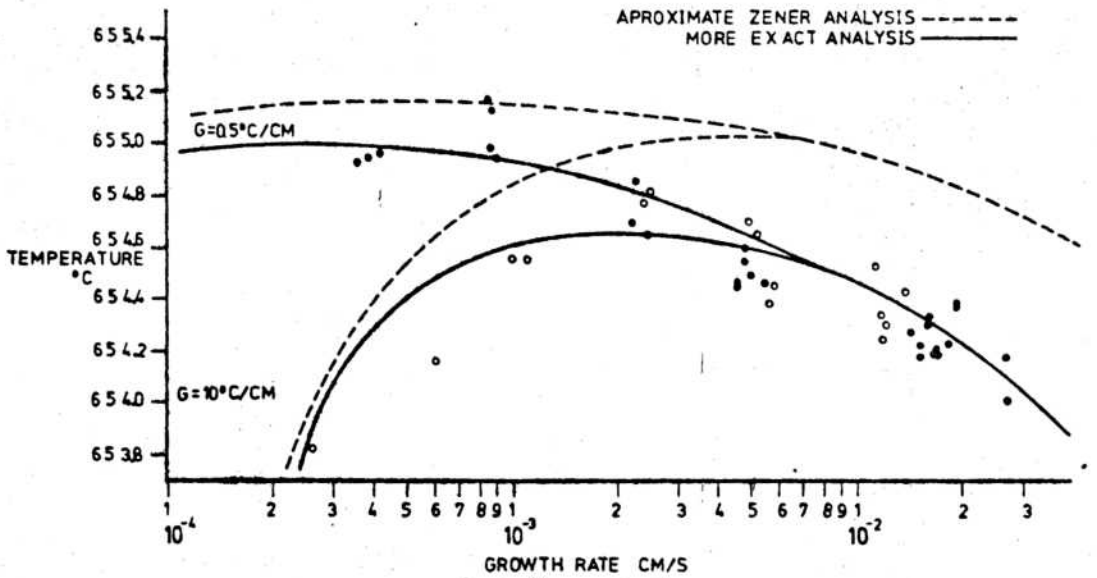

Fig. 2. A comparison between experiment and theory in Al–2%Cu alloy using an expanded temperature scale to illustrate the behaviour of the two analyses at high velocities and two temperature gradients. From ref. [8].

The interface temperature can be considered as the result of three effects:
(a) the matching of the composition variation between the dendrites to the average gradient ahead of the interface;
(b) an additional radial gradient;
(c) the undercooling due to curvature.

The analysis of eq. (4) shows that ΔT:
(i) at low growth rates depends strongly on G_L;
(ii) at high growth rates fundamentally depends on the solidification speed R.

Fig. 2, corresponding to Burden and Hunt's work [8], gives a comparison between experiment and theory in Al–2%Cu, using an expanded temperature scale to illustrate the behaviour of the two theoretical analysis [8] for two gradient values. Recent work by Tassa and Hunt [11] uses the much simpler Zener analysis which is also used in the present work.

In order to obtain a general expression of local distribution of solute, a mass balance is made in the elemental volume of fig. 1. For a solidified amount $(-df_L)$ in a time dt and for A_0 = area of the elemental volume transversal to the heat flow:

Solute increase in liquid = (Solute rejected at interface) + (Net flow of solute by diffusion in liquid) – (Solute back diffusion in solid), (5)

$$\gamma_L(A_0 f_L\, dx)\, dC_L/dt = -\gamma_L(C_L - C_S)\, A_0\, dx\, df_L/dt + d/dx(D_L \gamma_L A\, \partial C_L/\partial x)\, dx - D_S A_0/L\, dx\, \gamma_L\, dC_S/dy\,, \quad (6)$$

where γ_L = liquid density, D_S = solid diffusion coefficient, and $L = \lambda/2$ = half of the cellular spacing.

Additional suppositions:
(i) No macrosegregation exists. The solute balance in the liquid, in front of the liquid isotherm is:

$$R(C_t - C_\infty) = -D_L\, \partial C_L/\partial x\,. \quad (7)$$

Taking into consideration eq. (1),

$$\partial C_L/\partial x = (R/D_L)(a - b)\,. \quad (8)$$

The solute gradient is an average value considered as valid for the interdendritic liquid.
(ii) The liquid lateral area is $A = A_0 f_L$, then

$$\partial A/\partial x = A_0\, \partial f_L/\partial x\,. \quad (9)$$

(iii) The solidification is in the steady state condition

$$\partial f_L/\partial x = -R^{-1}\, \partial f_L/\partial t\,. \quad (10)$$

Replacing eqs. (8), (9) and (10) in eq. (1), and sim-

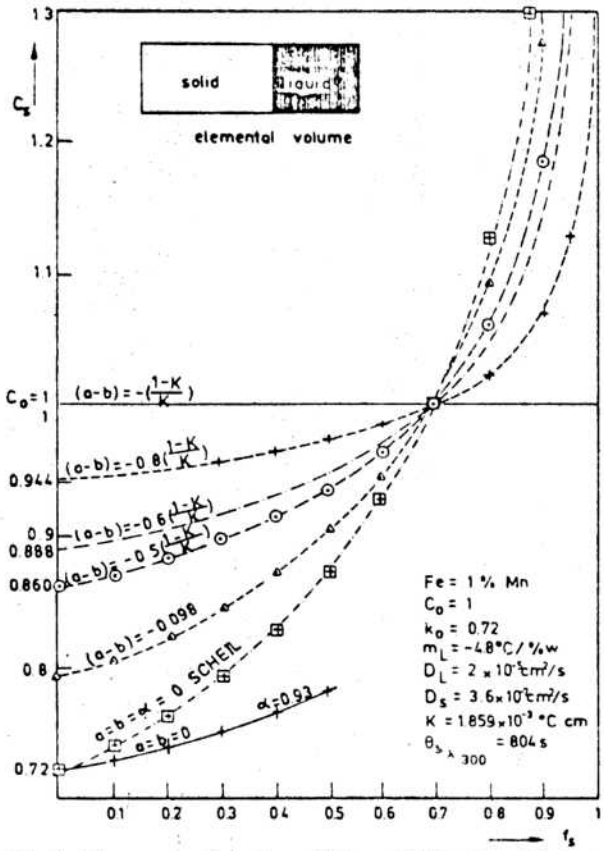

Fig. 3. Microsegregation in cellular solidification when a Fe–1%Mn alloy is considered. The solute distribution into an elemental volume according to eq. (16) and different values of the parameters a and b is shown.

plifying A_0, γ_L and dx,

$$f_L \frac{dC_L}{dt} = -(C_L - C_S)\frac{df_L}{dt} - (a-b)\,C_\infty \frac{df_L}{dt} - \frac{D_S}{L}\frac{dC_S}{dy}. \quad (11)$$

(iv) The rate of wall thickening is constant

$$dy/dt = L/\theta_S, \quad (12)$$

where θ_S = local solidification time, and from eq. (12), considering that $C_S = k_0 C_L$, defining

$$\alpha = D_S\theta_S/L^2 = 4D_S\theta_S/\lambda^2, \quad (13)$$

and reordering, we get:

$$\frac{df_L}{f_L + \alpha k_0} = \frac{dC_L}{C_L(1-k_0) + (a-b)\,C_\infty}. \quad (14)$$

Integrating the first term between 1 and f_L, and the second between C_t and C_L, and taking into account that $f_L = 1 - f_S$ and $C_L = C_S/k_\theta$,

$$C_S = k_0 C_0\left[\frac{a-b}{k_0-1} + \left(\frac{C_t}{C_\infty}\frac{a-b}{k_0-1}\right)\left(1 - \frac{f_S}{1+\alpha k_0}\right)^{k_0-1}\right]. \quad (15)$$

This expression corresponds to the solid composition at the interface during the solidification for each solid fraction f_S as a function of the alloy properties: D_L, D_S, k_0 and m_L, the growth conditions: G_L and R and the tip composition C_t. Considering expression (1), the general expression for local distribution is obtained:

$$C_S = k_0 C_0\left[\frac{a-b}{k_0-1} + \left(1 - \frac{(a-b)\,k_0}{k_0-1}\right) \times \left(1 - \frac{f_S}{1+\alpha k_0}\right)^{k_0-1}\right]. \quad (16)$$

Fig. 3 corresponds to $C_S = f(f_S)$ for different values of a and b when an Fe–1%Mn alloy is considered.

3. Discussion

The general expression (16) can be considered for particular cases

(i) When $a = b = \alpha = 0$ the Scheil equation (12) of solute distribution is obtained

$$C_S = k_0 C_0 (1 - f_S)^{k_0 - 1}. \quad (17)$$

If $a = b = 0$ and $\alpha \neq 0$:

$$C_S = k_0 C_0\left(1 - \frac{f_S}{1+\alpha k_0}\right)^{k_0-1}. \quad (17')$$

(ii) When $a \neq 0$ and $b = \alpha = 0$ the expression corresponds to that developed by Bower, Brody and Flemings [13]

$$C_S = k_0 C_0\left[\frac{a}{k_0-1} + \left(1 - \frac{ak_0}{k_0-1}\right)(1-f_S)^{k_0-1}\right]. \quad (18)$$

If $a \neq 0$, b and $\alpha \neq 0$:

$$C_S = k_0 C_0\left[\frac{a}{k_0-1} + \left(1 - \frac{ak_0}{k_0-1}\right)\left(1 - \frac{f_S}{1+\alpha k_0}\right)^{k_0-1}\right]. \quad (18')$$

Fig. 3-23 from ref. [6] shows cellular microsegregation according to eq. (18) for an Al–4.5%Cu alloy. At the limit of $a = 0$, the result is exactly the same as obtained by applying eq. (17). Even at high values of a, substantial eutectic change is predicted. Thus the expression accounts for the detection of high segregation at the nodes of the substructure, a fact experimentally observed, even at very low solute concentration [14–17]. The Burden and Hunt analysis shows that b will be negligible for low growth rate, while a grows in importance for low growth rates and high liquid gradients. As a consequence eq. (18) will respond quite well for those conditions which exist in general for cellular growth.

3.1. Cellular dendritic solidification

The cellular type of solidification can be extended to cooperative dendritic growth or cellular dendrites, considering a plate morphology. This assumption has experimental support for alloys having cubic [2,13] or hexagonal crystallography [18]. According to Flemings [6] cellular dendritic solidification occurs for a low relationship between G_L and R. In these circumstances, $a \to 0$ fundamentally as a consequence of the low value of D_L ($\sim 10^{-5}$ cm^2/s). Then, it seems to be correct to consider in eq. (16), $a = 0$. If no solid diffusion is considered, $\alpha = 0$ and eq. (16) becomes:

$$C_S = k_0 C_0 \left[\frac{-b}{k_0 - 1} + \left(1 + \frac{bk_0}{k_0 - 1} \right) (1 - f_S)^{k_0 - 1} \right]. \quad (19)$$

If solid back diffusion is considered, $\alpha \neq 0$:

$$C_S = k_0 C_0 \left[\frac{-b}{k_0 - 1} + \left(1 + \frac{bk_0}{k_0 - 1} \right) \times \left(1 - \frac{f_S}{1 + \alpha k_0} \right)^{k_0 - 1} \right] \quad (19')$$

When ingot solidification is considered, the parameter b has only importance at the beginning of the solidification due to the high R value. For the rest of the ingot b is negligible and eq. (19) tends to the Scheil equation. Then, eq. (19) could be considered as applicable to high rate solidification processes; for example, welding. In this particular process the solidification begins by epitaxial growth from the base metal, with high liquid gradient and low growth rate. The growth rate increases until the welding axis; there is a maximum. As a consequence, near the base metal, eq. (18) would respond better for the segregation profile; while at the weld axis, eq. (19) would be applicable.

3.2. Dendrite arm spacing

The solute redistribution model considered is independent of the arm spacing. According to Flemings the dendrite arm spacing is a function of the temperature gradient and the growth rate [6]. Thus the relationship between λ and G and R is

$$\lambda = c(GR)^{-n} \quad (20)$$

where c is a constant depending of the alloy composition and the exponent n is:
$n = 1/3$ for secondary arm spacing,
$n = 1/2$ for primary arm spacing.

3.3. Diffusion in the solid

Although Brody and Flemings [10] extended the treatment considering the diffusion in the solid from melting temperature to room temperature, the parameter α only takes into account the diffusion during the solidification process. Flemings and coauthors do not consider the parameter b in any circumstance and considered that the microsegregation in unidirectional solidification and columnar growth is described by eq. (17').

On the other hand, considering that eq. (13) connects the local solidification time with the dendrite arm spacing, and taking into account that λ is a function of θ_S [6], Brody [19] suggests that if the parameter α does not vary with a change in the dendrite arm spacing the segregation ratio S does not depend on the rate of cooling. As a consequence, an electron beam welding structure and an ingot structure would have the same degree of segregation. Without entering into considerations about arm spacing as a function of the local solidification time pointed out by Weinberg [20], we point out that the general eq. (16) indicates that the local composition does not depend only on α but also on the parameters a and b. These two parameters will change with the solidification rate as well as with the gradient into the liquid.

3.4. Segregation ratio

Eq. (4) can be expressed as:

$$\Delta T = G_L D_L / R + BR^{1/2} . \quad (21)$$

In fig. 4 the limits of the diagram are given by the plane S–L interface. This is, where no constitutional supercooling exits, and for a diffusionless transformation where the solid obtained has a liquid composition. In both cases the segregation ratio

$$S = C_{S\,max}/C_{S\,min} = 1 .$$

Taking into account expression (20), eq. (21) becomes:

$$\Delta T = (c/\lambda)^{1/n} \frac{D_L}{R^2} + BR^{1/2} . \quad (22)$$

Fig. 4 shows the segregation ratio obtained for different local rates of freezing, arm spacing and thermal gradients. In order to rationalize the results it is necessary to take into account that for a diagram of the type presented at fig. 1, $C_{max} = C_E$ = const. Then, an increase in ΔT gives a higher value of C_{min} and as a consequence S decreases. Thus, from fig. 4 it can be concluded that for a given value of C_0:
(i) for low solidification rates, below 10^{-3} cm/s, and gradients higher than 10°C/cm, it is possible to obtain cellular dendrite substructures with a low segregation ratio and variable arm spacing;
(ii) for solidification rates below 10^{-3} cm/s and for the same arm spacing, the segregation ratio increases when the gradient decreases;
(iii) for high solidification rates, higher than 10^{-2} cm/s and for the same solidification rate, it is possible to obtain different arm spacings characterized by the same segregation ratio.

If for given conditions of G_L and R, C_0 increases, the tip undercooling ΔT will increase, and taking into account that $C_{max} = C_E$ = const., S will decrease. These conditions could be extrapolated to the analysis of welding solidification. In fact, according to the preceding concepts the microsegregation ratio will change from the base metal according to diagrams (ΔT, G, R, λ). Experiments in Al–Cu are under way [21] but experimental results by Edvarsson et al. [22] in steels indicate that microprobe measurements show that the concentration at the middle of a dendrite arm increases with increasing solidification rate. The same authors affirm that: (i) a dramatic increase in the solidification rate implies that conditions corresponding to diffusionless solidification are obtained as a consequence $S = 1$, and (ii) during the transition from dendritic to diffusionless solidification, the degregation will decrease. These results are therefore in agreement with the predictions of the model proposed.

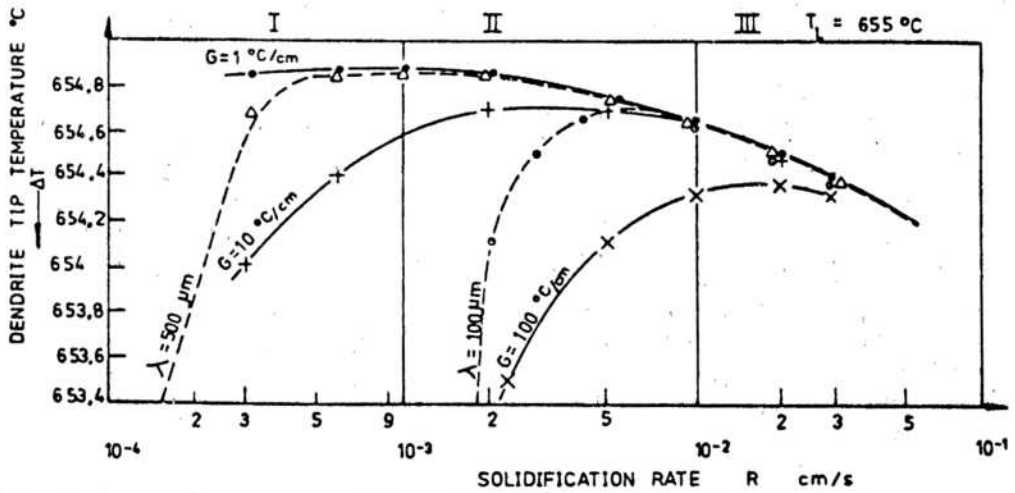

Fig. 4. Relationship between the temperature of the tip of a dendrite and the rate of solidification for different values of G_L and arm spacing. The figure shows the regions of maximum and minimum segregation.

4. Summary and conclusions

As Flemings pointed out [6], the actual morphology of the dendrites is much more complex than the simple plate-like or cylindrical morphology generally used for calculations involving solid diffusion. Thus, a detailed description of the solute distribution in the cellular dendritic substructure requires numerical solutions of the diffusion equation that take into account the more complex morphology, coarsening effects, etc. However, expression (16) will provide a simplified solution for microsegregation. The particular cases of that equation constitute acceptable approaches to the reality, under different conditions:

(i) Expressions (18) or (18′) for cellular microsegregation leading to node segregation.

(ii) Expressions (17′) and (17) for columnar growth when the solidification rate is not important and the solid back diffusion is or is not taken into consideration.

(iii) Expressions (19) or (19′) when R is important, such as at the beginning of the columnar grains of an ingot, or at the axis of a welding. In this process the region near the base metal will be better described by expressions (18) or (18′).

(iv) For processes where the rate of solidification changes through the process, as in welding, the segretation ratio would depend for each alloy considered on diagrams of "$\Delta T, G, R, \lambda$" type.

Acknowledgements

To the Multinational Program of Metallurgy OAS–CNEA and to the Comisión de Investigaciones de la Provincia de Buenos Aires (CIC) for partial support.

References

[1] M.C. Flemings, Sheffield Intern. Conf. on Solidification and Casting, Sheffield, 1977.
[2] G. Horvay and J.W. Cahn, Acta Met. 9 (1961) 695.
[3] G.F. Bolling and W.A. Tiller, J. Appl. Phys 32 1961, 2587.
[4] D.E. Temkin, Soviet Phys-Dokl. 5 (1960) 609.
[5] R. Trivedi, Acta Met. 18 (1970) 287.
[6] M.C. Flemings, Solidification Processing (McGraw-Hill, New York, 1974).
[7] M.H. Burden and J.D. Hunt, J. Crystal Growth 22 (1974) 99.
[8] M.H. Burden and J.D. Hunt, J. Crystal Growth 22 (1974) 109.
[9] M.H. Burden and J.D. Hunt, J. Crystal Growth 22 (1974) 328.
[10] H.D. Brody and M.C. Flemings, Trans TMS-AIME 236 (1966) 615.
[11] M. Tafsa and J.D. Hunt, J. Crystal Growth 34 (1976) 38.
[12] E. Scheil, Z. Metallk. 34 (1942) 70.
[13] T.F. Bower, H.D. Brody and M.C. Flemings, Trans TMS-AIME 236 (1966) 624.
[14] H. Biloni, Can. J. Phys., 39 (1961) 497.
[15] H. Biloni and G.F. Bolling, Trans TMS-AIME 227 (1963) 1361.
[16] H. Biloni, G.F. Bolling and G.S. Cole, Trans TMS-AIME 233 (1965) 251.
[17] H. Biloni, G.F. Bolling and H.A. Domian, Trans TMS-AIME 233 (1965) 177.
[18] M.A. Audero and H. Biloni, J. Crystal Growth 18 (1973) 257.
[19] H.D. Brody, Solidification Technology (Brood Hill, 1974) p. 53.
[20] F. Weinberg and R.K. Buhr, The Solidification of Metals (ISI P 110, 1968) p. 295.
[21] H. Palacio, M. Solari and H. Biloni, to be published.
[22] T. Edvarsson, H. Fredriksson and I. Svensson, Metal Sci. (Sept. 1926) 298.